Article

Cell Reports

hnRNPU is required for spermatogonial stem cell pool establishment in mice

Graphical abstract

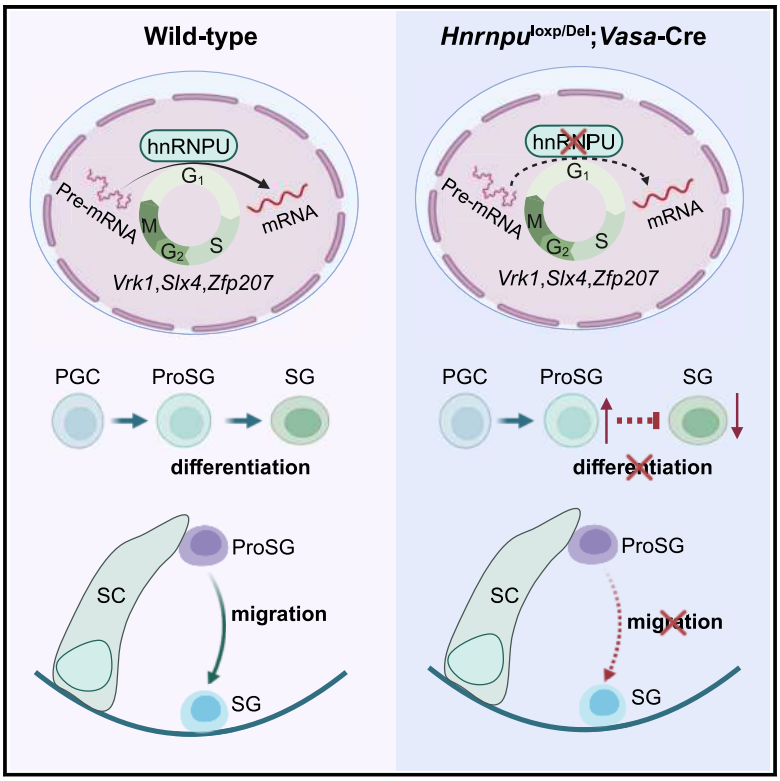

Highlights

- hnRNPU expression traverses germ-cell development and is abundant in perinatal germ cells
- hnRNPU regulates the establishment of the SSC pool and is essential for male fertility
- Loss of hnRNPU causes ProSG-to-SG transition failure and Sertoli-cell-only syndrome in mice
- hnRNPU modulates alternative splicing of cell-cycle-related genes in male germ cells

Authors

Yujiao Wen (文玉娇), Shumin Zhou (周淑敏), Yiqian Gui (桂以倩), ..., Keren Cheng (程柯仁), Xiaoli Wang (王晓莉), Shuiqiao Yuan (袁水桥)

Correspondence

shuiqiaoyuan@hust.edu.cn

In brief

Wen et al. report that loss of hnRNPU results in failure to establish a spermatogonial stem cell pool, leading to Sertoli-cell-only syndrome. Single-cell RNA sequencing revealed that ProSG-to-SG transitions are disturbed in *Hnrnpu*-deficient mice. hnRNPU affects the migration and differentiation of ProSG by regulating alternative splicing of cell-cycle-related genes.

Wen et al., 2024, Cell Reports *43*, 114113
April 23, 2024 © 2024 The Author(s). Published by Elsevier Inc.
https://doi.org/10.1016/j.celrep.2024.114113

CellPress

Cell Reports

CellPress
OPEN ACCESS

Article

hnRNPU is required for spermatogonial stem cell pool establishment in mice

Yujiao Wen (文玉娇),[1,2,8] Shumin Zhou (周淑敏),[1,8] Yiqian Gui (桂以倩),[1,8] Zeqing Li (李泽卿),[3,8] Lisha Yin (尹丽莎),[1,8] Wenchao Xu (徐文超),[1,4] Shenglei Feng (丰胜磊),[1,5] Xixiang Ma (马西祥),[1,5] Shiming Gan (甘世明),[1] Mengneng Xiong (熊孟能),[1] Juan Dong (董娟),[2] Keren Cheng (程柯仁),[6] Xiaoli Wang (王晓莉),[1] and Shuiqiao Yuan (袁水桥)[1,5,7,9,*]

[1]Institute of Reproductive Health, Tongji Medical College, Huazhong University of Science and Technology, Wuhan 430030, China
[2]Department of Obstetrics and Gynecology, Union Hospital, Tongji Medical College, Huazhong University of Science and Technology, Wuhan 430022, China
[3]School of Nuclear Technology and Chemistry & Biology, Hubei University of Science and Technology, Xianning 437100, China
[4]Department of Urology, Tongji Hospital, Tongji Medical College, Huazhong University of Science and Technology, Wuhan 430030, China
[5]Laboratory of Animal Center, Huazhong University of Science and Technology, Wuhan 430030, China
[6]Center for Reproductive Medicine, The Fourth Affiliated Hospital, Zhejiang University School of Medicine, Yiwu 322000, China
[7]Shenzhen Huazhong University of Science and Technology Research Institute, Shenzhen 518057, China
[8]These authors contributed equally
[9]Lead contact
*Correspondence: shuiqiaoyuan@hust.edu.cn
https://doi.org/10.1016/j.celrep.2024.114113

SUMMARY

The continuous regeneration of spermatogonial stem cells (SSCs) underpins spermatogenesis and lifelong male fertility, but the developmental origins of the SSC pool remain unclear. Here, we document that hnRNPU is essential for establishing the SSC pool. In male mice, conditional loss of hnRNPU in prospermatogonia (ProSG) arrests spermatogenesis and results in sterility. hnRNPU-deficient ProSG fails to differentiate and migrate to the basement membrane to establish SSC pool in infancy. Moreover, hnRNPU deletion leads to the accumulation of ProSG and disrupts the process of T1-ProSG to T2-ProSG transition. Single-cell transcriptional analyses reveal that germ cells are in a mitotically quiescent state and lose their unique identity upon hnRNPU depletion. We further show that hnRNPU could bind to *Vrk1*, *Slx4*, and *Dazl* transcripts that have been identified to suffer aberrant alternative splicing in hnRNPU-deficient testes. These observations offer important insights into SSC pool establishment and may have translational implications for male fertility.

INTRODUCTION

In mammals, spermatogonial stem cells (SSCs) can self-renew to maintain a relatively constant number and differentiate to produce functional sperm.[1,2] SSCs are derived from prospermatogonia (ProSG; also named as gonocyte), a limited, transient cell type that is poorly understood.[3] According to mitotic activity, morphology, and anatomical position, ProSG can be divided into three types: multiplying ProSG (M-ProSG), primary transitional ProSG (T1-ProSG), and secondary transitional ProSG (T2-ProSG).[4,5] In mice, accompanied by sex differentiation, M-ProSG is derived from primordial germ cells (PGCs) and forms the initial ProSG. M-ProSG generates T1-ProSG and enters a mitotically silent state. In neonatal mice, T1-ProSG restores the cell cycle and converts to T2-ProSG, a precursor of SSCs that can migrate from the center of the lumen to the basement membrane of seminiferous tubules.[3,6] Following the migration, ProSG gives rise directly to both undifferentiated spermatogonia and differentiating spermatogonia around postnatal day 3 (P3) to P5, whereby the former becomes the SSC pool in favor of lifelong male fertility while the latter engages in the first wave of spermatogenesis.[7–9] Defects in SSC pool establishment usually result in Sertoli-cell-only syndrome (SCOS) and male sterility.[10–13] The establishment of the SSC pool or the transition from ProSG to SSC is dependent on many factors. Although several studies have shown that a transcriptional factor (RHOX10) and epigenetic factor (JMJD1A and JMJD1B) could transcriptionally regulate the ProSG-to-SSC transition,[10,11,14] highlighting the importance of genetic factors in the SSC establishment, we currently know only the tip of the iceberg of how ProSG transforms into SSC.

In addition, a hallmark of ProSG is the perinatal mitotic arrest that occurs prior to postnatal spermatogonial transition.[15] After birth, ProSG differentiates into SSC or differentiating spermatogonia and migrates from the center of seminiferous tubules to the basement membrane.[6,16] Along with the migration and differentiation process, ProSG re-enters the cell cycle. At present, further elucidation is needed regarding the importance of mitotic activity in the differentiation and migration process of ProSG and the regulatory mechanisms of cell cycle re-entry.

This is an open access article under the CC BY-NC-ND license (http://creativecommons.org/licenses/by-nc-nd/4.0/).

The heterogeneous nuclear ribonucleoprotein (hnRNP) family is a group of RNA-binding proteins with more than 20 hnRNP members from A to U. In addition to the classical role of hnRNPs in binding to nascent mRNA, the functions of hnRNPs in various biological processes have been successively confirmed, such as DNA transcription, pre-mRNA alternative splicing, mRNA stability, and protein translation.[17] Notably, hnRNPs have been found to be highly expressed in male germ cells.[18] Our previous study characterized one of hnRNP family members, hnRNPU, as a co-transcription factor that interacts with WT1 and SOX9 and regulates the transcription of *Sox8/9* in mouse Sertoli cells.[19] However, the role of hnRNPU in SSC establishment remains unknown.

In this study, we report that hnRNPU is highly expressed in perinatal ProSG and spermatogonia and regulates the migration of spermatogonia to the basement membrane for establishing SSC pools. In male mice, genetic deficiency of hnRNPU in ProSG causes defects in the migration of ProSG toward the SSC niche, leading to SCOS and male infertility. Interestingly, single-cell RNA sequencing (scRNA-seq) analysis outcomes identify three known germ-cell subtypes during perinatal male germ-cell development. Germ cells emerge along a trajectory path from ProSG to undifferentiate spermatogonia and differentiate spermatogonia, mirroring the chronological order of perinatal spermatogenesis. In the absence of *Hnrnpu* expression, ProSG in a mitotically quiescent state fails to restore mitotic activity, thereby disrupting the process of ProSG-to-SSC transition. This study highlights the essential role of hnRNPU in establishing the SSC pool and facilitating male germ-cell differentiation to ensure male fertility.

RESULTS

hnRNPU expression traverses germ-cell development and is highly expressed in spermatogonia

Because we previously identified that hnRNPU was highly expressed in mouse Sertoli cells and male germ cells,[19] we assessed the cellular localization of hnRNPU in P56 mouse male germ cells to explore the role of hnRNPU during spermatogenesis. The result showed that hnRNPU was highly expressed in the nucleus of spermatogonia, pachytene spermatocytes, and round spermatids in the seminiferous tubules (Figures S1A and S1B). Further mRNA expression analysis of the *Hnrnpu* gene in purified testicular cells confirmed that hnRNPU was highly expressed in spermatogonia and pachytene spermatocytes (Figure 1A). To further clarify the cellular localization of hnRNPU during male germ lineage development, we examined the expression of hnRNPU perinatally in mouse testes at different time points, including embryonic day 12.5 (E12.5), E15.5, E18.5, P3, P7, and P56, and found that hnRNPU was continuously expressed during germ-cell development and localized in the nucleus of PGCs, ProSG, spermatogonia (SG), and spermatocytes (Figure 1B). Consistent with the above results, we found that hnRNPU was also expressed in the nucleus of both fetal and adult human germ cells (Figure 1C). To depict the function of hnRNPU in spermatogonial differentiation, we examined its expression levels in undifferentiated SG and differentiating SG. The results showed that hnRNPU was expressed in both undifferentiated SG and differentiating SG (Figures 1D, 1E, and S1C–S1E). Together, these data indicated that hnRNPU is expressed throughout the male germline, including fetal, neonatal, and adult germ cells and localized in the nucleus of ProSG, undifferentiated SG, and differentiating SG (Figure 1F).

Ablation of hnRNPU in ProSG leads to Sertoli-cell-only syndrome in mice

To investigate the role of hnRNPU in early male germ-cell development, we bred the *Vasa*-Cre mouse line with the previously described *Hnrnpu*$^{flox/flox}$ mouse line[19] to obtain *Vasa*-Cre; *Hnrnpu*$^{flox/Del}$ conditional knockout mice (herein designated as Vasa-Cre-cKO or cKO). PCR-based genotyping analyses of mouse tail and isolated germ cells confirmed the genotype of Vasa-Cre-cKO (*Vasa*-Cre; *Hnrnpu*$^{flox/Del}$), heterozygous control (*Hnrnpu*$^{+/flox}$), and wild-type (WT) (*Hnrnpu*$^{+/+}$) mice genetically (Figure 2A). Immunofluorescence (IF) assays revealed that hnRNPU was specifically lost in DDX4-positive germ cells in Vasa-Cre-cKO testes at P3, whereas hnRNPU was expressed in the germ cells of littermate controls, indicating that hnRNPU was successfully knocked out in male germ cells (Figure 2B). Further analysis revealed that both mRNA and protein expression levels of hnRNPU were significantly decreased in Vasa-Cre-cKO testes compared to the control testes (Figures 2C and 2D).

Subsequently, fertility tests revealed that both Vasa-Cre-cKO male and female mice were completely infertile (Figure 2E). Consistent with these sterile phenotypes, both testes and ovaries of Vasa-Cre-cKO mice at P56 were morphologically significantly smaller than controls, and the number of DDX4-positive germ cells in testes and ovaries was also dramatically decreased in Vasa-Cre-cKO mice (Figures 2F and S1F–S1G). In addition, the ratio of testis weight to body weight of Vasa-Cre-cKO mice remarkably reduced from P7 compared with the control (Figure 2G). Histologic analyses documented that germ cells were gradually lost from P5, and rarely or no germ cells were present in the seminiferous tubules at P10 (Figure 2H). Moreover, no mature sperm were detected in the epididymides, and the testicular cross-sections had only a layer of Sertoli cells remaining near the basement membrane of the seminiferous tubules in adult Vasa-Cre-cKO mice (Figures 2I and 2J), which resembled the SCOS of human infertility.

hnRNPU is essential for establishing the SSC pool

To determine when spermatogonial proportion changed in Vasa-Cre-cKO mice, we performed immunostaining of DDX4 with PLZF on testicular cross-sections at P1 to P7. The results showed that the number of both PLZF-positive cells (undifferentiated SG) and DDX4-positive cells (germ cells) were comparable between Vasa-Cre-cKO testes and control testes at P1–P3 while appearing to be reduced significantly from P5 (Figures 3A–3C, S1H, and S1I), suggesting that the proportion of undifferentiated SG affected in the testis of Vasa-Cre-cKO mice began by P5. In addition, c-KIT-positive differentiating SG was also significantly decreased in Vasa-Cre-cKO mouse testes at P7 compared with controls (Figures 3D and 3E). We then stained for Ki67 (a proliferation marker) to explore the reasons for the loss of spermatogonia. We found that the percentage of Ki67- and PLZF-double-positive cells per PLZF-positive spermatogonia was decreased in Vasa-Cre-cKO

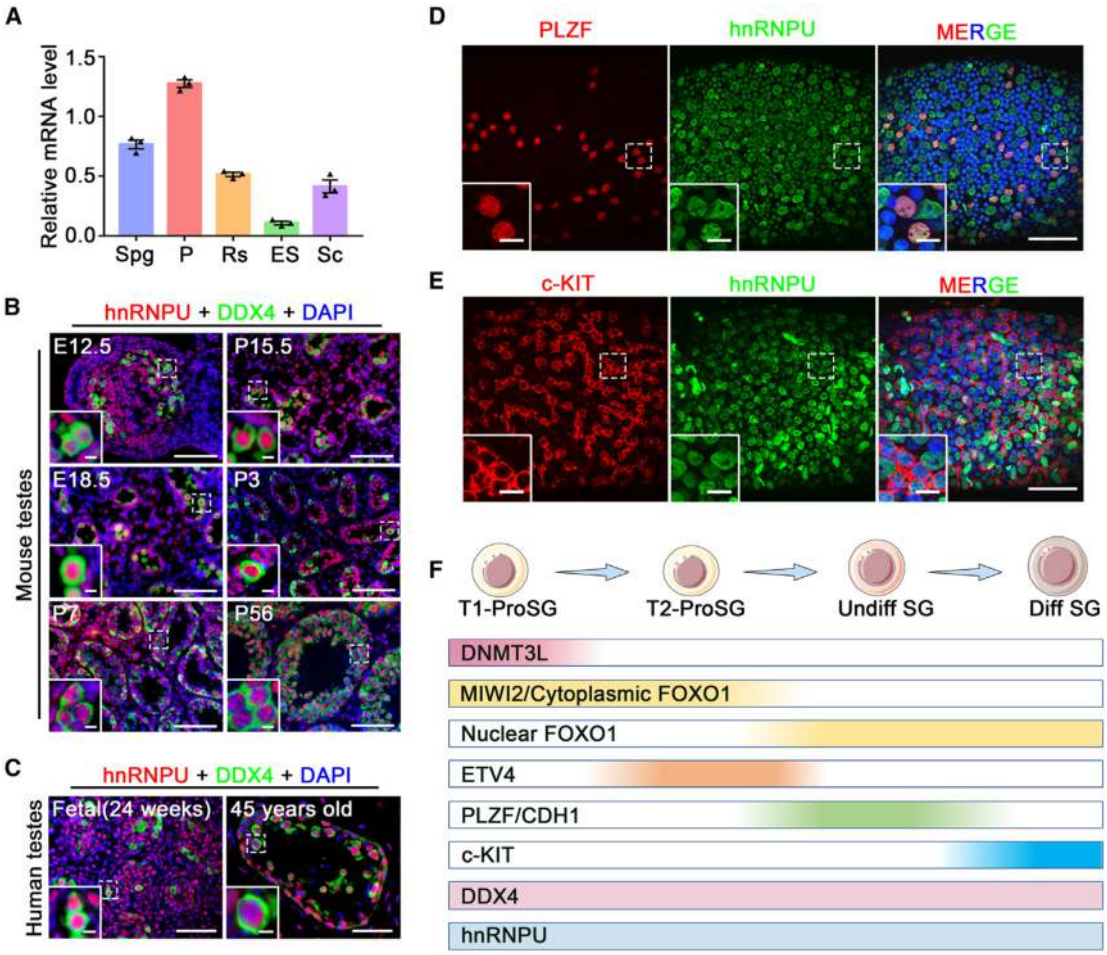

Figure 1. hnRNPU is expressed throughout the male germline

(A) mRNA level of hnRNPU in the isolated mouse spermatogenic cells and Sertoli cells from mouse testes at P56, analyzed by RT-qPCR. *n* = 3 independent biological replicates from different mice. Spg, spermatogonia; P, pachytene; Rs, round spermatids; ES, elongating spermatids; Sc, Sertoli cells.

(B) Cross-section of mouse testis with immunostaining for hnRNPU (red) and germ-cell marker DDX4 (green) at embryonic day 12.5 (E12.5), E15.5, E18.5, postnatal day 3 (P3), P7, and P56. *n* = 3 biologically independent genital ridges or testes from three different mice. Scale bars, 50 μm. Inset scale bars, 5 μm.

(C) Immunofluorescence of hnRNPU (red) and DDX4 (green) in human fetal testis (24 weeks post conception) and obstructive azoospermia patient testis (45 years old). Scale bars. 50 μm. Inset scale bars, 5 μm.

(D and E) Whole-mount immunostaining of P56 testes with hnRNPU antibody with PLZF (D) and c-KIT (E), respectively. Enlarged panels show the expression of hnRNPU in PLZF-positive undifferentiated spermatogonia and c-KIT-positive differentiating spermatogonia. *n* = 3 biologically independent testes from three different mice. Scale bars, 50 μm. Inset scale bars, 5 μm.

(F) Schematic depicting the expression profile of commonly used markers for prospermatogonia (ProSG) and spermatogonia (SG). hnRNPU is ubiquitously expressed within primary transitional T1-ProSG, T2-ProSG, Undiff SG, and Diff SG populations. T1-ProSG, primary transitional ProSG; T2-ProSG, secondary transitional ProSG; Undiff SG, undifferentiated spermatogonia; Diff SG, differentiating spermatogonia.

testes compared to controls at P3 and P5 (Figures 3F and 3G). Further analysis by TUNEL staining revealed that the apoptosis of spermatogonia was most prominent in Vasa-Cre-cKO mice at P5 (Figures S1J and S1K). These results indicate that the homeostasis of proliferation and apoptosis was disturbed in Vasa-Cre-cKO undifferentiated SG.

To investigate whether hnRNPU directly impacts the maintenance of SSCs, we generated *Hnrnpu*$^{flox/flox}$;*Ddx4*-Cre^{ERT2} male mice for tamoxifen-induced hnRNPU deletion in germ cells (referred to as iKO) and collected the testes from control and iKO mice (35 days post tamoxifen injection) for analyses (Figure S2A). In iKO mice, the testis size, ratio of testis/body weight, and sperm number were all decreased (Figures S2B–S2D), and periodic acid-Schiff (PAS) staining displayed severe spermatogenic defects with germ-cell loss and multinuclear cell appearance (Figure S2E). The co-staining of PLZF or GFRa1 using iKO testis cross-sections showed that undifferentiated SG (including SSCs) still existed and that the number of undifferentiated SG was comparable between iKO and control testes, suggesting the dispensable role of hnRNPU in SSC maintenance (Figures S2F–S2I). Taken together, our data indicate that hnRNPU is essential for SSC pool establishment but not for SSC maintenance.

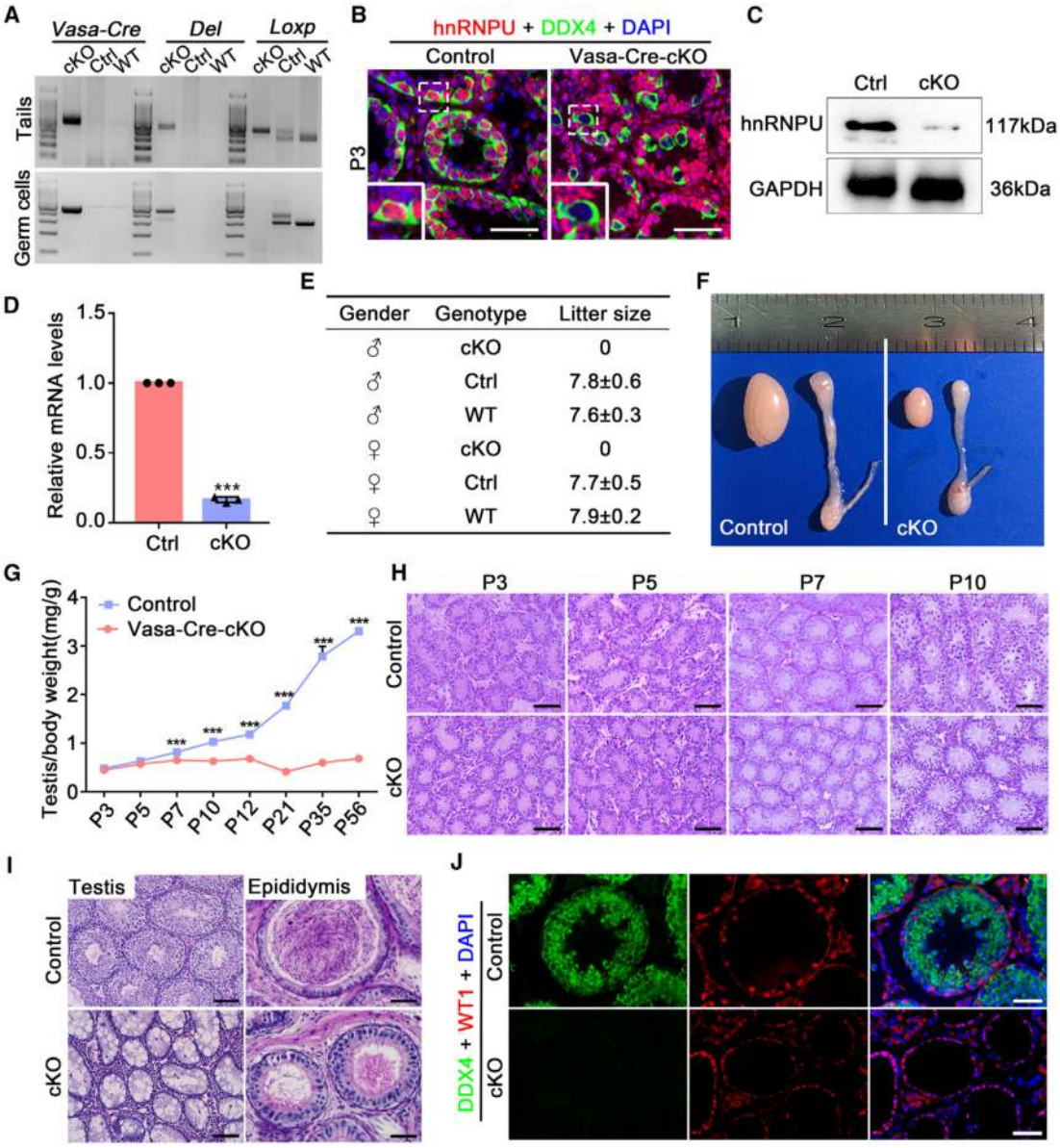

Figure 2. Essential role of hnRNPU in spermatogenesis and male fertility

(A) Representative PCR genotyping images of tails and germ cells from cKO (*Vasa-Cre*; *Hnrnpu*$^{flox/Del}$), Ctrl (control, *Hnrnpu*$^{+/flox}$), and WT (wild-type) mice are shown.

(B) Representative immunofluorescent images indicate that hnRNPU (red) was successfully knocked out in DDX4-positive (green) germ cells of Vasa-Cre-cKO mice at P3. Scale bars, 50 μm.

(C) Representative western blot images of hnRNPU protein in Ctrl and cKO germ cells at P3 are shown. GAPDH served as a loading control.

(D) RT-qPCR analyses reveal that the mRNA expression level of hnRNPU was significantly reduced in cKO testes at P3. Data are presented as mean ± SEM, $n = 3$ biologically independent mice for each genotype; ***$p < 0.001$.

(E) Quantification of the average number of pups per litter in cKO, Ctrl, and WT mice. Data are presented as mean ± SEM, $n = 3$ biologically independent mice for each genotype.

(F) Gross morphology of testis and epididymis from Ctrl and cKO mice at P56.

(G) Comparison of testis weight per body weight ratio of control and Vasa-Cre-cKO mice from P3 to P56. Data are presented as mean ± SEM, $n = 3$ biologically independent mice for each genotype; ***$p < 0.001$.

(H) Testicular PAS staining of control and cKO mice at P3, P5, P7, and P10. Scale bars, 50 μm.

(I) Representative PAS staining images of testis and cauda epididymis from control and cKO mice at P56. Scale bar, 50 μm.

(J) Double immunofluorescence staining for Sertoli-cell marker WT1 (red) and germ-cell marker DDX4 (green) in control and cKO mouse testis sections at P56. Scale bars, 50 μm.

Data are representative of a minimum of three independent experiments and three biologically independent mice for each genotype.

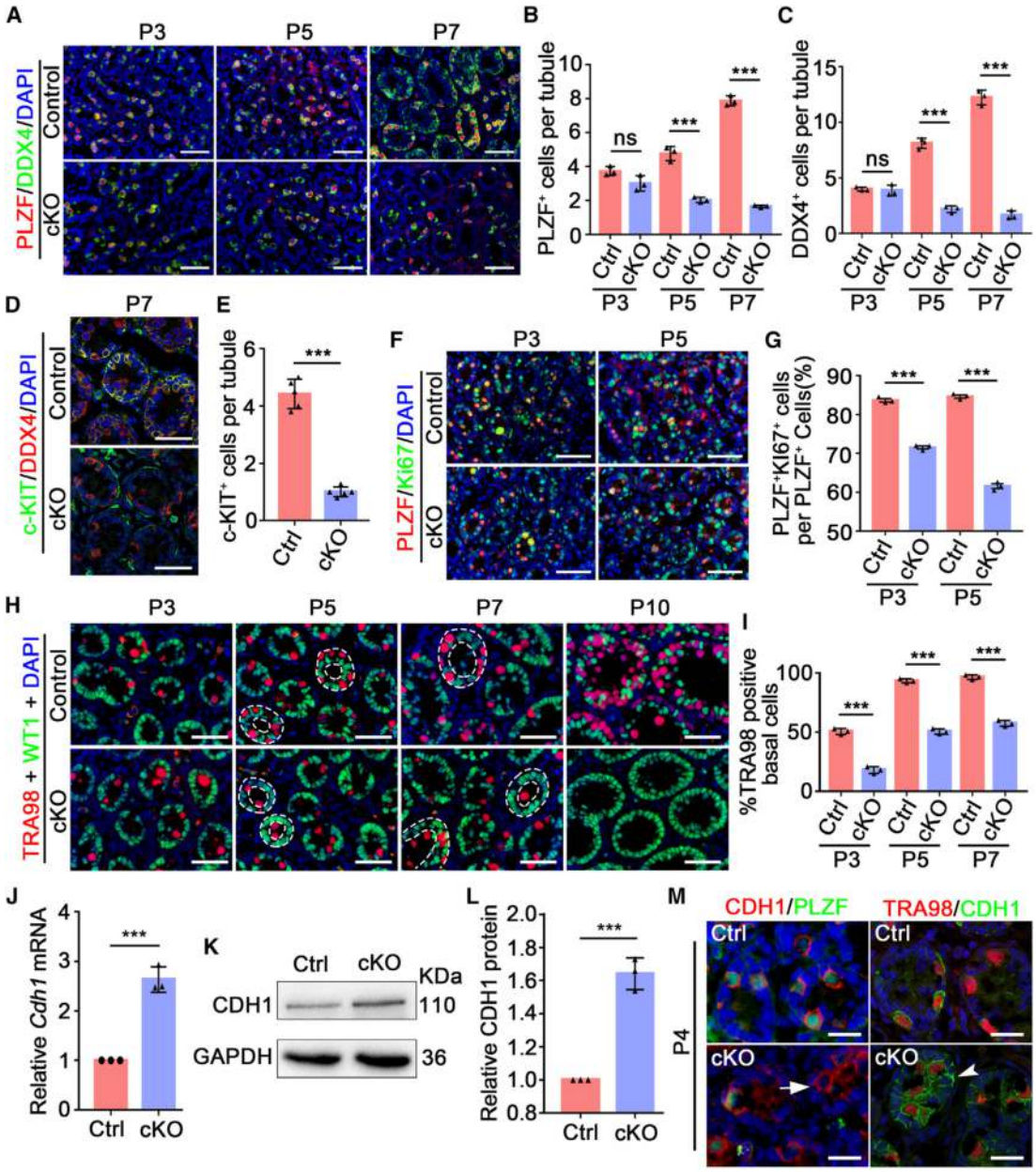

Figure 3. Establishment of SSC pool was disrupted in Vasa-Cre-cKO mice

(A) Representative co-immunofluorescent staining images for PLZF (red) and DDX4 (green) on control and cKO mouse testicular sections from P3, P5, and P7 mice, respectively. Scale bars, 50 μm.

(B) Quantification of PLZF-positive undifferentiated spermatogonia for (A). $n = 3$ biologically independent mice for each genotype. ns, not significant; ***$p < 0.001$.

(C) Quantification of DDX4-positive undifferentiated spermatogonia for (A) is shown. $n = 3$ biologically independent mice for each genotype. ns, not significant; ***$p < 0.001$.

(D) Representative immunofluorescent images of c-KIT (green) co-stained with DDX4 (red) in control and cKO mouse testes at P7. Scale bars, 50 μm.

(E) Quantification of c-KIT-positive differentiating spermatogonia for (D). $n = 5$ biologically independent mice for each genotype. ***$p < 0.001$.

(F) Representative immunofluorescent images of co-staining PLZF (red) with proliferation marker Ki67 (green) in control and cKO mouse testicular sections at P3 and P5, respectively. Scale bars, 50 μm.

(G) Histogram showing the proportion of Ki67 and PLZF double-positive proliferating undifferentiated spermatogonia in the PLZF-positive cells in (F). Data are presented as mean ± SEM, $n = 3$ biologically independent mice for each genotype; ***$p < 0.001$.

(H) Representative immunofluorescent images of co-staining TRA98 (red) and Sertoli-cell marker WT1 (green) in control and cKO mouse testes at P3, P5, P7, and P10, respectively. Dashed lines indicate germ cells located in the center and periphery of seminiferous tubules. Scale bars, 50 μm.

(legend continued on next page)

hnRNPU is required for ProSG migration

Because ProSG needs to migrate toward the basement membrane and establish the SSC pool around P3–P5,[4,7–9] we examined the efficiency of ProSG migration to the basal membrane of seminiferous tubules in Vasa-Cre-cKO mice. In control mice, interestingly we found that about 50% of germ cells migrated to the basement membrane of seminiferous tubules at P3 and that almost all germ cells had completed the migration and were adjacent to the basement membrane at P5, while all spermatogonia intermixed with Sertoli cells to locate on the basement membrane at P7 (Figures 3H and 3I). However, in Vasa-Cre-cKO mice, germ cells were trapped in the center of the seminiferous tubules from P3 to P7 in comparison to control mice (Figures 3H and 3I), suggesting the aberrant migration of ProSG from the center to the peripheral basement membrane of seminiferous tubules occurred. Since CDH1 (also known as E-cadherin) is a cell-adhesion factor and marker of undifferentiated SG and its ectopic expression is associated with the frustrating migration process of ProSG,[13,20] we speculated that the deregulation of CDH1 contributes to a disrupted migration process of ProSG in Vasa-Cre-cKO mice. As expected, both mRNA and protein expression levels of CDH1 in Vasa-Cre-cKO testes at P4 were significantly higher than that of the control testes (Figures 3J–3L). Notably, we found that CDH1 is only expressed in PLZF germ cells in the control testis cross-sections at P4, whereas CDH1 is ectopically expressed in TRA98-negative cells (somatic cells) in Vasa-Cre-cKO testes (Figure 3M). Together, these results suggest that hnRNPU is essential for ProSG migration and that loss of hnRNPU in ProSG leads to an aberrant and ectopic expression of CDH1 in the testes.

Ablation of hnRNPU in ProSG affects the ProSG fate decision

Given that ProSG failed to migrate to the SSC niche in Vasa-Cre-cKO mice, we asked whether the differentiation of ProSG and the efficiency of ProSG-to-spermatogonia transition are disturbed in Vasa-Cre-cKO mouse testes. It has been reported that ProSG and spermatogonia can be distinguished according to the subcellular localization of FOXO1, which is when ProSG are transformed into spermatogonia and FOXO1 is transported from the cytoplasm to the nucleus.[21] To quantify this process, we examined both the percentage of spermatogonia that share a nuclear localization of FOXO1 (nFOXO1) and the percentage of ProSG that have a cytoplasmic localization of FOXO1 (cFOXO1). In the control testes, the percentage of spermatogonia (nFOXO1/nFOXO1 + cFOXO1) increased from 57% at P3 to 70% at P5, and the percentage of ProSG (cFOXO1/nFOXO1 + cFOXO1) decreased from 43% at P3 to 30% at P5 (Figures 4A and 4B). In Vasa-Cre-cKO testes, the percentage of nFOXO1$^+$ spermatogonia is about 31% at P3, 38% at P4, and 39% at P5, which is significantly lower than that in control testes (Figures 4A and 4B). Correspondingly, the percentage of cFOXO1$^+$ ProSG in Vasa-Cre-cKO testes is remarkably higher than the control testes (Figures 4A and 4B). Further, we isolated the cytoplasm and nucleus protein of control and Vasa-Cre-cKO germ cells and found that the nuclear-to-cytoplasm ratio of FOXO1 was significantly decreased in Vasa-Cre-cKO germ cells (Figures S3A and S3B), indicating that ProSG failed to transit into spermatogonia and accumulated in Vasa-Cre-cKO testes. In support of these observations, we co-stained MIWI2, a recognized marker for ProSG,[22] with TRA98 to further visualize the defects of ProSG-to-spermatogonia transition. Consistent with the findings, the number of MIWI2-positive ProSG was comparable at P1 and began to increase from P3 in Vasa-Cre-cKO testes compared with controls. At P5, MIWI2-positive ProSG were absent in control testes but still present in Vasa-Cre-cKO testes, confirming that the transition of ProSG to spermatogonia is blocked in Vasa-Cre-cKO mice (Figures 4C and 4D). These results show that the deletion of hnRNPU in ProSG leads to the accumulation of ProSG and the reduction of spermatogonia.

Since T1-ProSG are inactive spermatogonia in the mitotic arrest state, which begin to transform into T2-ProSG at P1 and can proliferate, migrate, and differentiate into spermatogonia,[2,23] we sought to investigate whether the differentiation process from T1-ProSG to T2-ProSG is disrupted. To this end, we used the recently identified T1-ProSG marker DNMT3L to perform IF staining of Vasa-Cre-cKO mouse testes at P1, P3, and P5.[2,24] In control mice, all TRA98-positive germ cells were DNMT3L-positive T1-ProSG at P1, about 49.53% of germ cells in the testes of control mice were DNMT3L-positive at P3, and DNMT3L-positive T1-ProSG disappeared at P5 (Figures 4E and 4F). Interestingly, in Vasa-Cre-cKO mice, the ratio of DNMT3L/TRA98 double-positive cells per total TRA98-positive cells was comparable to that of littermate control mice at P1, indicating that the maintenance of T1-ProSG was normal (Figures 4E and 4F). At P3, DNMT3L-positive cells accounted for 71.67% of germ cells in the testes of Vasa-Cre-cKO mice, significantly higher than that of control mice (Figures 4E and 4F). At P5, a more pronounced difference occurred, with DNMT3L-positive T1-ProSG detectable in Vasa-Cre-cKO mice but not in control mice, indicating that T1-ProSG is blocked in their process of differentiation toward T2-ProSG upon hnRNPU deletion (Figures 4E and 4F). Moreover, consistent with the key characteristic of T1-ProSG in which germ cells were in a non-proliferative state, we found that the number of non-proliferative germ cells was comparable between Vasa-Cre-cKO and control testes at P1 (Figures S3C and S3D). To verify the T1- to T2-ProSG transition defects, we performed co-immunofluorescent staining of TRA98

(I) Quantification of the ratio of basal germ cells (TRA98$^+$) in control and cKO group for (H). % TRA98 positive basal cells = (TRA98-positive germ cells located at the basement membrane/total TRA98-positive germ cells) × 100%. Data are presented as mean ± SEM, $n = 3$ biologically independent mice for each genotype; $^{***}p < 0.001$.

(J) RT-qPCR shows that mRNA levels of *Cdh1* are significantly elevated in cKO testes at P4. Data are presented as mean ± SEM, $n = 3$ biologically independent mice for each genotype; $^{***}p < 0.001$.

(K) Western blot indicates CDH1 protein levels in Ctrl and cKO testes at P4.

(L) Quantitative analysis of CDH1 protein levels in Ctrl and cKO testes. Data are presented as mean ± SEM, $n = 3$ biologically independent mice for each genotype; $^{***}p < 0.001$.

(M) Representative immunofluorescent images of testicular sections from Ctrl and cKO mice at P4 stained for CDH1, PLZF, and TRA98. Arrow indicates PLZF-negative and CDH1-positive cells. Arrowheads indicate TRA98-negative somatic cells with ectopic cytoplasmic CDH1 expression. Scale bars, 20 μm.

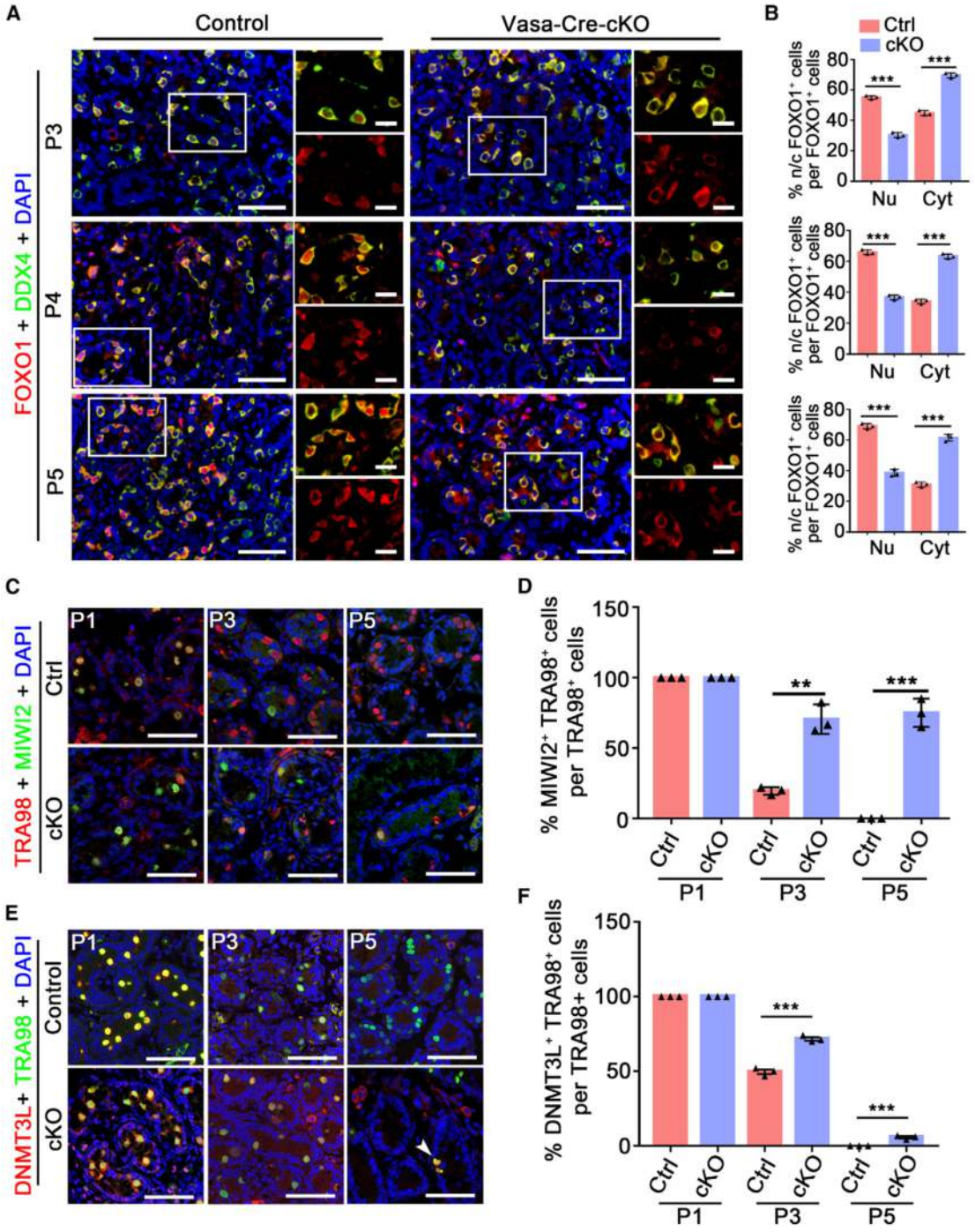

Figure 4. hnRNPU deficiency disrupts the process of ProSG-to-spermatogonia transition

(A) Representative co-immunofluorescent staining images for the FOXO1 and DDX4 on control and Vasa-Cre-cKO mouse testes from P3, P4, and P5 mice, respectively. Scale bars, 50 μm. Enlarged panels on right show the merged channels of FOXO1 (red) and DDX4 (green). Inset scale bars, 10 μm.

(B) Quantifications of the percentage of ProSG and spermatogonia for (A). The percentage of ProSG and spermatogonia was calculated by using the following formula: % ProSG = cytoplasmic FOXO1$^+$ cells/total FOXO1 $^+$ cells; % spermatogonia = nuclear FOXO1$^+$ cells/total FOXO1$^+$ cells. Nu, nuclear; Cyt, cytoplasmic. Data are presented as mean ± SEM, $n = 3$ biologically independent mice for each genotype; ***$p < 0.001$.

(C) Representative co-immunofluorescent staining images for the MIWI2 (green) and TRA98 (red) on control and cKO mouse testes from P1, P3, and P5 mice. Scale bars, 50 μm.

(D) Quantifications of the percentage of MIWI2-positive ProSG for (C). The ratio of ProSG was calculated as MIWI2- and TRA98-positive cells/total TRA98-positive cells. Data are presented as mean ± SEM, $n = 3$ biologically independent mice for each genotype; **$p < 0.01$, ***$p < 0.001$.

(legend continued on next page)

with ETV4, a recently identified marker for T2-ProSG.[2] The results showed that the percentage of ETV4-positive cells was decreased in Vasa-Cre-cKO in P4 testes, confirming that T1-ProSG failed to restore proliferation in Vasa-Cre-cKO mice (Figures S3E and S3F). Together, these data demonstrate that hnRNPU is required for the process of differentiation and transition of ProSG to spermatogonia.

scRNA-seq defines the defects during ProSG-to-SG transition in Vasa-Cre-cKO mice

To detect molecular changes during the ProSG-to-SG transition process in Vasa-Cre-cKO mice, we performed scRNA-seq on whole testicular cells from control and Vasa-Cre-cKO testes at P5. Subsequent analysis was based on control (9,674 cells) and Vasa-Cre-cKO (15,238 cells) datasets within 2,651 genes and 2,582 median genes detected per cell, respectively. Clustering analysis of the total cells from testes across all genotypes identified 23 major cell clusters (Figure S4A and Table S1). Control and Vasa-Cre-cKO testicular cells exhibited similar cell distributions, and testicular cells of these two genotypes were evenly distributed in each cluster (Figure S4B). To assign the cell types of each cluster, we used previously reported testicular markers: germ cells (*Dazl*, *Ddx4*), Sertoli cells (*Amh*, *Wt1*, *and Sox9*), Leydig cells (*Hsd3b1*, *Cyp11a1*), peritubular myoid cells (*Acta2*, *Myh11*), stroma cells (*Wnt5a*), macrophage cells (*Cd68*, *Lyz2*), and endothelial cells (*Pecm1*, *Esam*)[2,25–27] (Figures S4C and S4D). Followed by the analyses, a total of seven known types of testicular cell clusters and one unknown cluster were identified (Figure S4E). Moreover, scRNA-seq revealed that hnRNPU was ubiquitously expressed in all types of testicular cells, including germ-cell and somatic-cell clusters (Figure S4F), consistent with its expression pattern at the protein level (Figure 1). The proportions of testicular cell subtypes were counted separately to detect the differences between control and Vasa-Cre-cKO testicular cells. The results showed that the number of germ cells was reduced in Vasa-Cre-cKO mouse testes compared with controls (Figures S4G and S4H). Interestingly, the unknown cells were increased in Vasa-Cre-cKO testicular cells compared with the controls (Figures S4G and S4H), suggesting that some cells lost their unique identity upon hnRNPU ablation in germ cells.

To better clarify the cellular heterogeneity of germ cells, re-clustering analysis was performed on germ-cell clusters (including clusters 6, 9, and 10), and a total of seven subgroups (clusters 0–6) of germ cells was identified (Figure S5A); 99.4% of reclustered cells are located in clusters 1–5, while cluster 6 contains only 0.6% of reclustered cells and is separated from clusters 0–5 (Figure S5A). Further analysis revealed that a germ-cell marker (*Dazl*) was detected in clusters 0–5 and not in cluster 6, indicating that cluster 6 might not be germ cells (Figure S5B). Thus, cluster 6 was removed and clusters 0–5 were used for the subsequent analyses (Figure 5A). In all, testicular cells of Vasa-Cre-cKO mice were mainly distributed in cluster 0, partially in clusters 1, 2, and 4, and rarely in cluster 3, indicating that the distribution of germ-cell subtypes was uneven between control and Vasa-Cre-cKO mouse testes (Figure 5B). Cluster 3 was characterized by markers of differentiating spermatogonia (e.g., *Dmrtb1*, *Kit*, *Rhox13*, *Stra8*, or *Dnmt3b*) and was tentatively classified as differentiating spermatogonia (Diff SG) (Figures 5C, 5D, and S5C). Undifferentiated spermatogonia (containing SSCs and progenitors) markers manifested expression peaks in cluster 4; thus, cluster 4 was named undifferentiated spermatogonia (Undiff SG) (Figures 5C, 5D, and S5C). Cells in clusters 0 and 5 were categorized as ProSG, expressing ProSG markers (e.g., *Id1*, *Id2*, *Klf4*)[24] with little or no detection of either Undiff SG markers (*Gfra1*, *Etv5*, *Nanos3*, *Egr4*, or *Neurog3*)[2,24,26,28] or Diff SG markers (*Dmrtb1*, *Kit*, *Rhox13*, *Stra8*, or *Dnmt3b*)[2,24,26] (Figures 5C, 5D, and S5C).

Since clusters 1 and 2 could not be defined by any of the known germ-cell subtype marker genes, we tentatively designated them as "transitional SG" according to their transcriptome signatures. Clusters 1 and 2 (transitional SG) shared similar transcriptome signatures of both Undiff SG and Diff SG (Figure 5E and Table S2). For instance, *Uchl1*, a marker gene for SSC,[29] was highly expressed in clusters 1 and 2 (Figure S5D). Further, the signature genes of clusters 1 and 2 (transitional SG) were enriched in gene ontology (GO) terms such as "metabolism of RNA," "chromatin organization," and "cell proliferation" (Figure S5E), suggesting that clusters 1 and 2 were involved in the regulation of cell proliferation. We then performed a pseudotime analysis based on the germ-cell cluster transcriptomes to mirror the chronological order of perinatally male gametogenesis. Germ cells emerged along a trajectory path from ProSG (clusters 0 and 5) to transitional SG (clusters 1 and 2) to Undiff SG (cluster 4) and Diff SG (cluster 3), suggesting that clusters 1 and 2 might act as the intermediate cell state during this process (Figures 5F, 5G, and S5F).

Interestingly, testicular cells from Vasa-Cre-cKO mice were more likely to be present in the early phase of the pseudotime trajectory characterized by the presence of ProSG and lost in late germ-cell clusters that represent spermatogonia (Figure 5H). Consistent with the above findings from IF analyses, a large proportion of Vasa-Cre-cKO germ cells were defined as ProSG (Figure 5I), suggesting that ProSG could not differentiate and triggered the accumulation of ProSG in the Vasa-Cre-cKO testes. Differentially expressed genes (DEGs) between control and Vasa-Cre-cKO for each cluster were then analyzed (Table S3). DEGs involved in cell-cycle regulation were among the top GO terms in the ProSG, transitional SG, and Undiff SG clusters (Figure S6A). In addition, GO analyses revealed that the reproductive process enriched for ProSG and transitional SG, germ-cell proliferation enriched for Undiff SG, and meiosis I enriched for Diff SG (Figure S6A), suggesting that the transcriptome network of the reproductive process was disturbed upon hnRNPU depletion in ProSG.

Considering that the cell cycle was disturbed in Vasa-Cre-cKO germ cells, germ cells were categorized as discrete cell-cycle

(E) Representative co-immunofluorescent staining images for the DNMT3L (red) and TRA98 (green) on control and cKO mouse testes from P1, P3, and P5 mice. Arrowhead indicates DNMT3L-positive cells in P5 cKO testes. Scale bars, 50 μm.
(F) Quantification of the percentage of T1-ProSG for (E). The percentage of T1-ProSG was calculated as both DNMT3L- and TRA98-positive cells/total TRA98-positive cells. Data are presented as mean ± SEM, representative of $n = 3$ biologically independent mice for each genotype; $^{***}p < 0.001$.

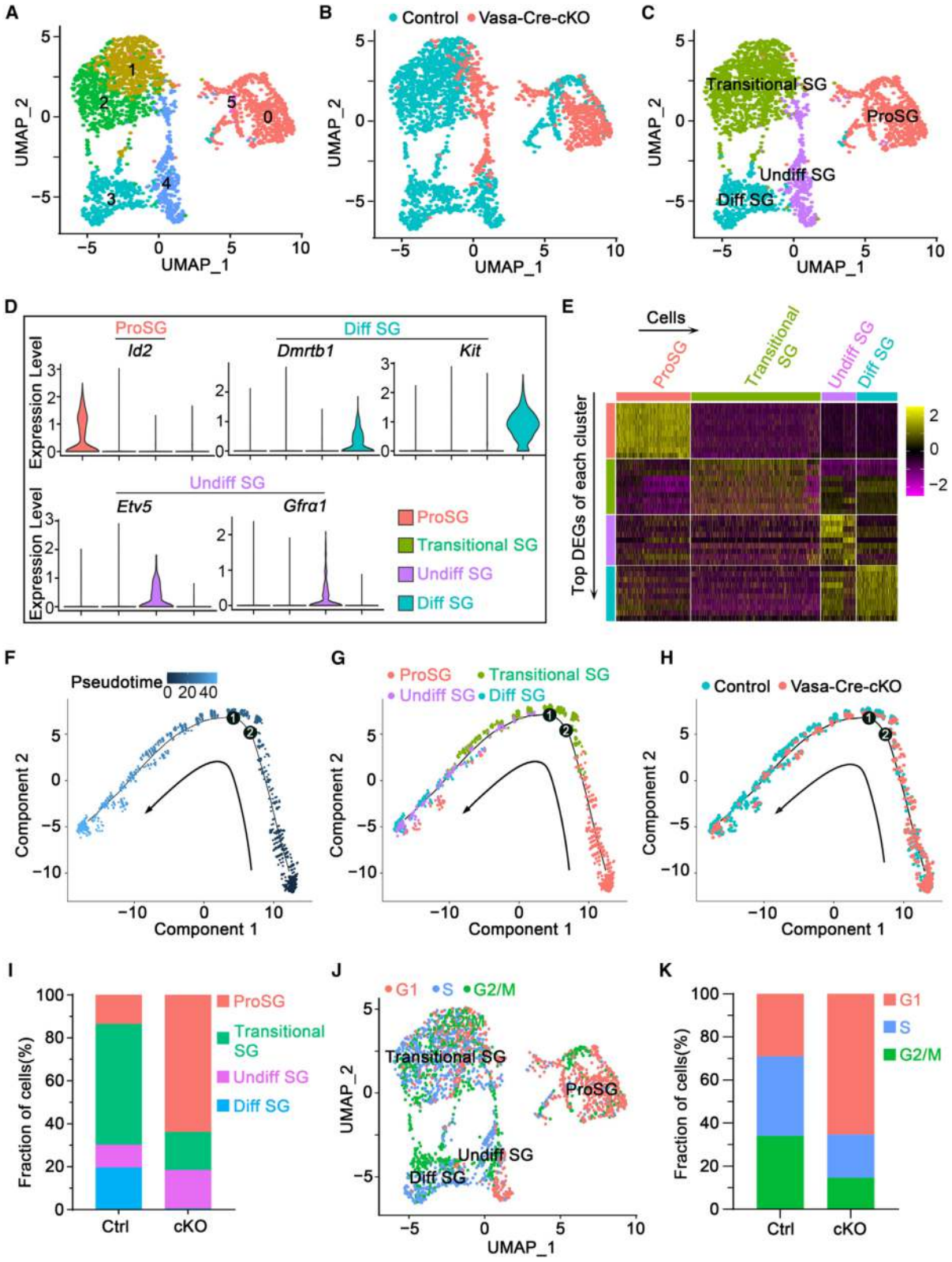

(legend on next page)

phases based on the uniform manifold approximation and projection (UMAP) plot to further describe their cell-cycle signature. We found that clusters 1 and 2 (transitional SG), cluster 4 (Undiff SG), and cluster 3 (Diff SG) were sorted into cell-cycle-active (G_1, S, or G_2/M) phases, while clusters 0 and 5 (ProSG) were in the G_1 state, indicative of G_0 arrest and quiescence (Figure 5J), suggesting that ProSG cluster was in cell-cycle quiescence and SG cluster was in a proliferative state. Subsequently, we performed a statistical analysis of the proportion of germ cells at each phase in the control and Vasa-Cre-cKO samples, respectively. The percentage of germ cells in G_1, S, and G_2/M phases was as follows (Ctrl vs. cKO): G_1 (28.9% vs. 65.4%), S (37.0% vs. 20.0%), G_2/M (34.1% vs. 14.6%) (Figure 5K). In Vasa-Cre-cKO germ cells, the proportion of germ cells in G_1 phase increased (Figure 5K), indicating that mitotic activation was hindered upon hnRNPU deletion and that germ cells were in a mitotically quiescent state.

hnRNPU regulates alternative splicing of cell-cycle-related genes

To fully understand the molecular mechanism of how hnRNPU regulates spermatogonial development, we performed RNA-seq on control and Vasa-Cre-cKO mouse testes at P4, at which time point the cell population is comparable between control and Vasa-Cre-cKO testes (Table S4). Compared to the testes of control mice, a total of 317 and 198 genes were identified as upregulated and downregulated, respectively, in the testes of Vasa-Cre-cKO mice (Figure S6B). GO-term analysis showed that the DEGs were mainly enriched in spermatogenesis, reproduction, cell migration, and cell differentiation (Figures S6C and S6D). Further, we analyzed the length of 3′ UTR and observed that the genes with dysregulated 3′ UTR were enriched in mRNA processing (Figures S6E and S6F), suggesting that hnRNPU might regulate the length of gene 3′ UTR.

Since hnRNPU could participate in alternative splicing (AS) events of precursor mRNA in tissues such as the heart,[30,31] we used rMATS software (replicate multivariate analysis of transcript splicing) to analyze the AS events from the RNA-seq data. The results showed that compared to the control group, 955 differentially AS events occurred in the testis of Vasa-Cre-cKO mice, most of which were skipped exon events, accounting for 79.5% (759 out of 955) of the total AS events (Figure 6A and Table S5). Other differentially AS events included mutually exclusive exon (153/955), alternative 5' splice site (14/955), alternative 3′ splice site (23/955), and retained intron (6/955) (Figure 6A and Table S5). Further, GO-term analysis revealed that genes with differentially AS events are enriched in the mitotic cell-cycle process (Figure 6B). Subsequently, we selected three genes (*Vrk1*, *Slx4*, and *Zfp207*) related to cell cycle to visualize based on RNA-seq analysis. Loss of hnRNPU resulted in differential expression of exon 13 in *Vrk1* (increased exon skipping), exon 3 in *Slx4* (increased exon skipping), and exon 9 in *Zfp207* (increased exon inclusion) (Figure 6C). Interestingly, we identified exon-skipping events at exon 8 of the *Dazl* gene (Figure 6C), a master translational regulator gene for spermatogonial development and spermatogenesis in mice.[32] PCR further confirmed these differentially AS events in testes and germ cells isolated from P4 testes (Figures 6D and S6G). In addition, we analyzed the RNA expression levels of *Vrk1*, *Slx4*, *Zfp207*, and *Dazl* and found no significant changes in the expression of these four genes (Figure S6H). Conclusively, these bioinformatics analyses suggest that hnRNPU could modulate the development of spermatogonia by regulating the gene network of spermatogonial development and alternative splicing of genes related to the cell cycle.

We next asked whether hnRNPU could bind to precursor mRNA in mouse germ cells. To this end, we performed RNA-binding protein co-immunoprecipitation coupled with sequencing (RIP-seq) in isolated germ cells from P4 testes to detect hnRNPU protein-bound RNA (Figures S7A and S7B). GO-term analyses revealed that hnRNPU-binding transcripts were enriched on cell cycle and cell division (Figure 7A). We further validated the enrichment of pre-mRNAs related to cell cycle and spermatogonial development, such as *Vrk1*,[33] *Slx4*,[34] *Dazl*,[32] *Ptpn11*,[35] *Ddx5*,[36,37] and *Dmrt1*.[38] RIP-qPCR and the peak diagram of RIP-seq indicated that hnRNPU binds to these six genes (Figures 7B, S7C, and S7D). Strikingly, *Vrk1*, *Slx4*, and *Dazl* also suffered alternative splicing (Figures 6C and 6D), indicating that hnRNPU might directly regulate the alternative splicing of *Vrk1*, *Slx4*, and *Dazl*.

Furthermore, the motif analyses showed that the mapped hnRNPU-binding sites are distributed among the intron regions (~38.99%) (Figure 7C), which was consistent with previous studies.[30,31] Interestingly, we also detected hnRNPU binding to exon (~27.98%) and 3′ UTR (24.06%) (Figure 7C). RNA-binding motif analysis revealed that hnRNPU preferred GU-, UGGG-, or GUUUU-rich tracts of RNA (Figure 7D), consistent with the characteristic of hnRNPU with high-affinity binding to G or U homopolymers.[30,31] Further analysis by comparing RNA-seq and RIP-seq data revealed that the transcripts of ~20.37% (166 out of 815) AS-changed genes were bound by hnRNPU, and

Figure 5. scRNA-seq defines aberrant ProSG-to-SSC progression in Vasa-Cre-cKO mice

(A) Reclustering analysis of combined control and Vasa-Cre-cKO germ cells projected onto UMAP plot.

(B) UMAP plots of individual libraries for germ cells isolated from control and Vasa-Cre-cKO testicular samples.

(C) UMAP plot shows clustering analysis of combined control and Vasa-Cre-cKO germ cells.

(D) Mean expression levels of ProSG, Diff SG, and Undiff SG marker genes to each cluster on the violin plots. Diff SG, differentiated spermatogonia; Undiff SG, undifferentiated spermatogonia.

(E) Heatmap showing the top differentially expressed genes (DEGs) of each cluster.

(F and G) Pseudotime ordering of combined control and Vasa-Cre-cKO mouse germ cells documented following the trajectory timeline of ProSG, Undiff SG, transitional SG, and Diff SG.

(H) Pseudotime trajectory analysis of control and Vasa-Cre-cKO mouse germ cells. cKO germ cells tend to be distributed early and decrease over time.

(I) Proportion of ProSG, transitional SG, Undiff SG, and Diff SG in control and Vasa-Cre-cKO samples.

(J) UMAP plot shows cell-cycle phase analysis of germ cells.

(K) Quantification of cells at each cell-cycle phase in Ctrl and cKO testicular cells.

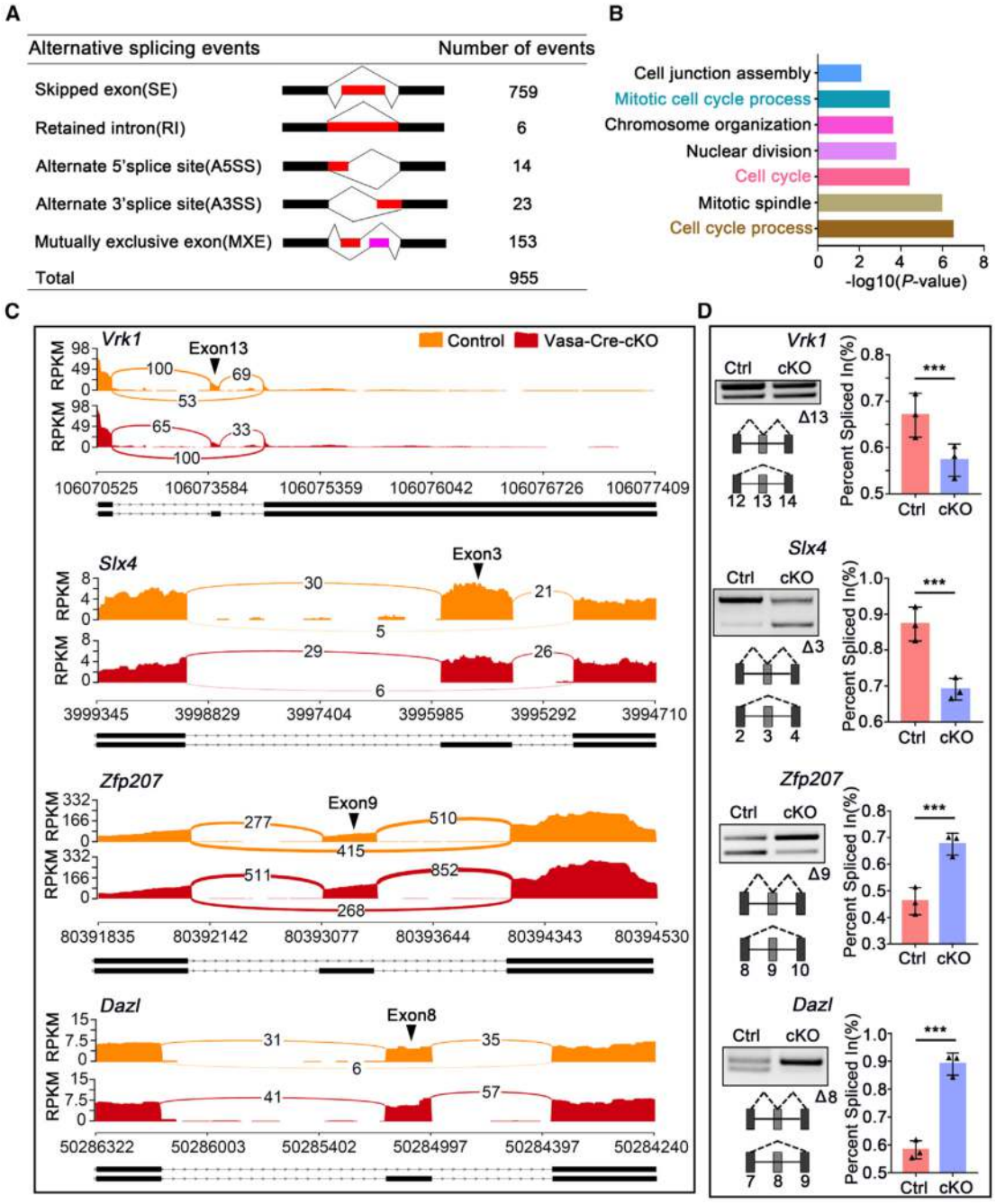

Figure 6. hnRNPU regulates alternative splicing post-transcriptionally

(A) Number of alternative splicing events occurring in Vasa-Cre-cKO testes at P4.

(B) GO-term enrichment analysis of genes with differentially alternative splicing events at P4.

(C) Sashimi plot showing differentially alternative splicing events of selected genes (*Vrk1*, *Slx4*, *Zfp207*, and *Dazl*) between control and Vasa-Cre-cKO mouse testes detected by RNA-seq.

(D) PCR validation of the selected candidate genes in isolated germ cells from P4 control and Vasa-Cre-cKO mice. Differentially spliced exons are denoted by "Δ*n*" (*n* being exon number). Below is a schematic representation of alternatively spliced exons. Bar plot on the right is the percentage of exons included (PSI), the values being expressed as mean ± SEM, $n = 3$ biologically independent mice for each genotype; ***$p < 0.001$.

these overlapping transcripts were enriched in cell migration, cell cycle, and cell division (Figures 7E and S7E). Interestingly, hnRNPU was also enriched on ~29.47% (183 out of 621) differentially expressed transcripts (Figure S7F), suggesting that hnRNPU also regulates gene expression in a splicing-independent mechanism.

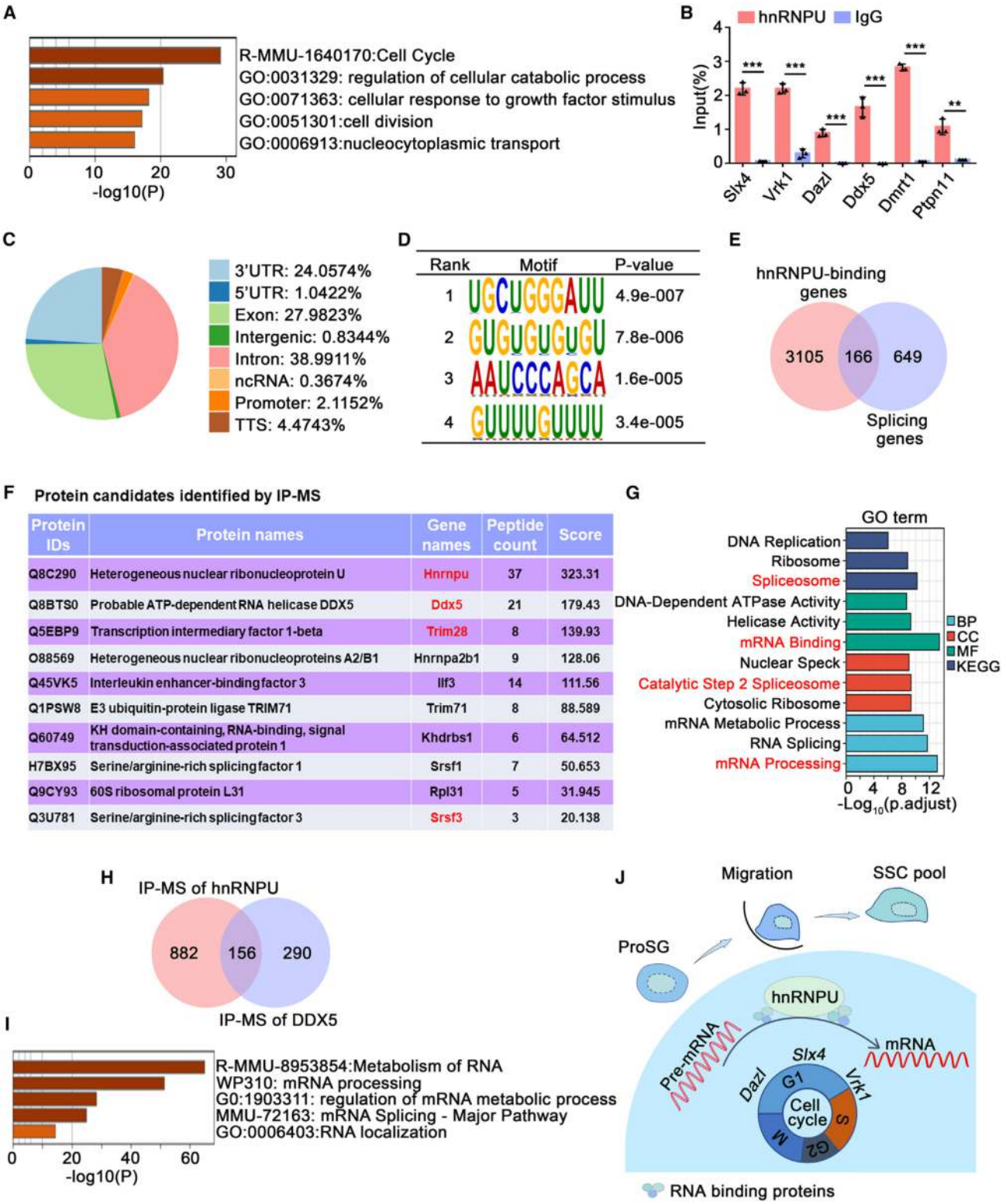

Figure 7. hnRNPU binds to pre-mRNA and interacts with RNA-binding proteins

(A) GO terms of hnRNPU-binding transcripts.

(B) RIP-qPCR shows that hnRNPU protein interacts with the mRNA of *Slx4*, *Vrk1*, *Dazl*, *Ddx5*, *Dmrt1*, and *Ptpn11* in isolated germ cells. Data are presented as mean ± SEM, $n = 3$ biological repeats; $^{**}p < 0.01$, $^{***}p < 0.001$.

(legend continued on next page)

To further elucidate the regulatory network of hnRNPU in spermatogonia development, we studied the hnRNPU-interactive protein network by reanalyzing our previous published immunoprecipitation-mass spectrometry (IP-MS) data from P5 mouse testes[19] and identified many hnRNPU candidate interaction proteins (Figure 7F). Further GO-term and Kyoto Encyclopedia of Genes and Genomes (KEGG) analysis of these interacting proteins showed that the top three pathways were mRNA binding, mRNA processing, and RNA splicing (Figure 7G). To verify the reliability of these interacting proteins identified by MS, we selected three proteins containing DDX5 (related to alternative splicing and spermatogonial development),[36,37] SRSF3 (related to alternative splicing and spermatogenesis),[39,40] and TRIM28 (related to spermatogonial development)[41] to perform co-immunoprecipitation coupled with western blot in isolated germ cells from P5 testes to confirm that hnRNPU does interact with these proteins in mouse germ cells (Figures S7G and S7H). Interestingly, previous studies have shown that DDX5 regulates the exon 8 skipping of *Dazl*,[36] which is consistent with the function of hnRNPU. Thus, we further analyzed the cooperation role between hnRNPU and DDX5. We compared IP-MS data of hnRNPU and DDX5 and found 156 common interacting proteins (Figure 7H). Further analysis revealed that these common interacting proteins were enriched in RNA metabolism, mRNA processing, regulation of mRNA metabolic process, mRNA splicing—major pathway, and RNA localization (Figure 7I). Altogether, these data indicate that hnRNPU could interact with RNA-binding protein and bind to precursor mRNA to regulate its alternative splicing during spermatogonial development (Figure 7J).

DISCUSSION

In our previous study, we conditionally knocked out hnRNPU in mouse Sertoli cells and observed that ablation of hnRNPU in Sertoli cells leads to severe testicular atrophy and failure of spermatogonia migration and proliferation.[19] In the current study, we demonstrated that loss of hnRNPU in germ cells leads to Sertoli-cell-only phenotype and that hnRNPU is able to regulate the differentiation and migration of ProSG and SSC pool establishment. Interestingly, knockout of hnRNPU in germ cells or somatic cells triggers similar phenotype defects in spermatogonial development. Additionally, loss of hnRNPU in Sertoli cells not only affects germ-cell development but also leads to rapid depletion of Sertoli cells, implying that hnRNPU in Sertoli cells is essential for both germ-cell and Sertoli-cell development. Sertoli cells sustain a relatively constant number in Vasa-Cre-cKO seminiferous tubules, indicating that hnRNPU in germ cells is not essential for the development of Sertoli cells. Therefore, the phenotype of germ-cell developmental defects observed in Sertoli-cell-specific knockout of hnRNPU mice possibly might occur due to the indirect effect of hnRNPU on spermatogenesis by affecting Sertoli-cell development and the spermatogenic microenvironment established by Sertoli cells. Consistently, germ-cell-specific or Sertoli-cell-specific knockout of *Aip1* could affect the migration of ProSG and spermatogonial maintenance,[13] which is similar to the regulatory role of hnRNPU during germ-cell development, suggesting that hnRNPU and AIP1 have a similar function in regulating spermatogenesis.

Of note, migration and cell-cycle changes are two important events during ProSG-to-spermatogonia transformation. In the current study, we found that hnRNPU-deficient ProSG failed to migrate to the basement membrane of seminiferous tubules to establish an SSC pool. This observation is consistent with recent studies reporting that intraluminal ProSG could converse to type A spermatogonia after injection of retinoic acid into the testis prior to migration.[42] It is worth noting that the number of undifferentiated spermatogonia and differentiating spermatogonia was reduced in Vasa-Cre-cKO mice, and no germ cells were observed in the seminiferous tubules at P10, indicating that the differentiation of T2-ProSG was disrupted and differentiating spermatogonia failed to enter the meiotic stage to become spermatocytes and ultimately fulfill the first wave of spermatogenesis. In addition, although ProSG in the center of seminiferous tubules can differentiate, they will undergo apoptosis,[43] and this was confirmed by TUNEL-staining analysis of Vasa-Cre-cKO mice.

Due to the high heterogeneity and low cell number of ProSG and Undiff SG, it is challenging to study their characteristics.[2,12] Although several studies have been devoted to distinguishing their subtypes and identifying some subtypes of ProSG and Undiff SG, much is still unknown about their subtypes.[2,24,44–47] In this study, we identified four cell types using the scRNA-seq technique: ProSG, transitional SG, Undiff SG, and Diff SG. It should be notated that clusters 1 and 2 could not be annotated by existing markers of germ-cell subtypes. By analyzing their highly variable gene, GO term, pseudotime trajectory, cell proportion, and cell cycle, we found their characteristics to be consistent with SG and thus were tentatively named transitional SG. Since ProSG resumes the cell cycle and transforms into SG after birth, we speculate that transitional SG may be a group of cells that have just resumed proliferation and have not yet fully transformed into Undiff SG or Diff SG. Interestingly, we also identified an unknown cluster, which is an independent cell type, accounting for 0.6% of the total germ cells. We tried to use a variety of marker genes to define it; however, the unknown cluster was

(C) Genomic distribution of hnRNPU-binding regions of transcripts.
(D) The four most enriched motifs identified from RIP-seq.
(E) Venn diagrams showing the overlap of hnRNPU-binding transcripts from RIP-seq and abnormal alternative splicing genes from RNA-seq.
(F) A list of ten hnRNPU-interacting candidates in mouse testes at P5 identified by IP-MS. Analysis is derived from our previous published data.[19]
(G) GO and KEGG enrichment analysis of hnRNPU-interacting proteins identified by IP-MS. hnRNPU-interacting proteins were mainly enriched on mRNA binding, mRNA processing, and spliceosome-related proteins.
(H) Venn diagrams showing the overlap of hnRNPU-binding proteins and DDX5-binding proteins from IP-MS.
(I) GO-term analyses of 156 overlapped binding proteins between DDX5 and hnRNPU.
(J) Model of hnRNPU-mediated gene regulation in ProSG and spermatogonia. hnRNPU functions as a post-transcriptional regulator, interacting with other RNA-binding proteins (such as DDX5 and SRSF3) to co-regulate the alternative splicing of *Vrk1*, *Slx4*, and *Dazl* for maintaining cell cycle in neonatal testes, thereby controlling ProSG fate decision.

not expressed germ-cell markers and weakly expressed stroma cell, peritubular myoid cell, and Sertoli-cell markers, suggesting that this cluster may comprise disturbed somatic cells. It is reasonable that a small proportion of unknown cells appear during testicular cell clustering because one recent article has also shown another/mixture of an unknown cluster in testicular scRNA-seq analyses.[48] For the analysis of AS using RNA-seq data generated from whole testes, we cannot rule out the technical limitation that the aberrant AS identified may be induced by the alteration of testicular cell subtypes. To eliminate the interference of somatic cells, we reverified the AS genes using isolated germ cells from Vasa-Cre-cKO and control mice at P4. Interestingly, AS abnormalities seem more obvious in germ-cell suspensions than in whole testes, which further confirmed that the aberrant AS of these genes is caused by the loss of hnRNPU rather than uneven cell subtypes.

In summary, our investigations introduce hnRNPU as a critical regulator and that hnRNPU drives the initial establishment of the SSC pool by promoting the migration of ProSGs into the SSC niche and their specific differentiation into SSCs. In this regard, hnRNPU conditional knockout mice could serve as an excellent model to study the process of ProSG-to-SSC transition. The findings in this study provide insights into the molecular mechanism that regulates SSC pool establishment and extends knowledge toward a better understanding of male germline stem cell biology, which may translate to the treatment of human male infertility.

Limitations of the study

In this study, we found that hnRNPU deficiency in mouse ProSG results in failure of ProSG differentiation and migration, leading to SCOS. Interestingly, we found that hnRNPU and DDX5 share 156 interacting proteins and that either hnRNPU or DDX5 may regulate exon 8 skipping of the *Dazl* gene. However, we cannot exclude that hnRNPU plays an important role in DNA transcription and other RNA metabolism-related events during the ProSG-to-SG transition process. Thus, it remains unknown whether other functions of hnRNPU in the ProSG-to-SG process are transcriptional or post-transcriptional. In addition, although the advent of single-cell sequencing technology has provided important clues to the definition of their subgroups, the classification of their subgroups is still controversial. Different sequencing methods, samples, and pipeline analyses can yield different results. Some sequencing methods themselves have limitations. For example, analysis using DDRTree in monocle2 often results in a few cells deviating from the cell clustering.

STAR★METHODS

Detailed methods are provided in the online version of this paper and include the following:

SUPPLEMENTAL INFORMATION

Supplemental information can be found online at https://doi.org/10.1016/j.celrep.2024.114113.

ACKNOWLEDGMENTS

We would like to thank Dr. Tom Maniatis at Columbia University College of Physicians and Surgeons for kindly sharing the *Hnrnpu*^{flox} mice and Dr. Deqiang Ding at Tongji University for kindly sharing the MIWI2 antibody with us. This work, in part, was supported by grants from the National Natural Science Foundation of China (82171605 and 82371625 to S.Y., 82101738 to J.D.), and the Basic Research Support Program of Huazhong University of Science and Technology (2023BR031).

AUTHOR CONTRIBUTIONS

S.Y., Y.W., and S.Z. conceived and designed the research. Y.W., S.Z., Y.G., Z.L., L.Y., W.X., S.F., X.M., S.G., M.X., J.D., K.C., and X.W. performed the bench experiments and data analyses. Y.G. and K.C. performed the bioinformatics analysis. Z.L. and Y.G. carried out the scRNA experiment and analysis. S.Z. and S.Y. wrote the manuscript. S.Y. supervised the project. All authors read and approved the manuscript.

DECLARATION OF INTERESTS

The authors declare no competing interests.

Received: July 20, 2023
Revised: January 28, 2024
Accepted: March 29, 2024

REFERENCES

1. de Rooij, D.G., and Grootegoed, J.A. (1998). Spermatogonial stem cells. Curr. Opin. Cell Biol. *10*, 694–701. https://doi.org/10.1016/s0955-0674(98)80109-9.
2. Tan, K., Song, H.W., and Wilkinson, M.F. (2020). Single-cell RNAseq analysis of testicular germ and somatic cell development during the perinatal period. Development *147*, dev183251. https://doi.org/10.1242/dev.183251.
3. Culty, M. (2009). Gonocytes, the forgotten cells of the germ cell lineage. Birth Defects Res. C Embryo Today. *87*, 1–26. https://doi.org/10.1002/bdrc.20142.
4. Culty, M. (2013). Gonocytes, from the fifties to the present: is there a reason to change the name? Biol. Reprod. *89*, 46. https://doi.org/10.1095/biolreprod.113.110544.
5. McCarrey, J.R. (2013). Toward a more precise and informative nomenclature describing fetal and neonatal male germ cells in rodents. Biol. Reprod. *89*, 47. https://doi.org/10.1095/biolreprod.113.110502.

6. Nagano, R., Tabata, S., Nakanishi, Y., Ohsako, S., Kurohmaru, M., and Hayashi, Y. (2000). Reproliferation and relocation of mouse male germ cells (gonocytes) during prespermatogenesis. Anat. Rec. *258*, 210–220. https://doi.org/10.1002/(SICI)1097-0185(20000201)258:2<210::AID-AR10>3.0.CO;2-X.

7. Manku, G., and Culty, M. (2015). Mammalian gonocyte and spermatogonia differentiation: recent advances and remaining challenges. Reproduction *149*, R139–R157. https://doi.org/10.1530/REP-14-0431.

8. Yoshida, S., Sukeno, M., Nakagawa, T., Ohbo, K., Nagamatsu, G., Suda, T., and Nabeshima, Y.i. (2006). The first round of mouse spermatogenesis is a distinctive program that lacks the self-renewing spermatogonia stage. Development *133*, 1495–1505. https://doi.org/10.1242/dev.02316.

9. Kluin, P.M., and de Rooij, D.G. (1981). A comparison between the morphology and cell kinetics of gonocytes and adult type undifferentiated spermatogonia in the mouse. Int. J. Androl. *4*, 475–493. https://doi.org/10.1111/j.1365-2605.1981.tb00732.x.

10. Kuroki, S., Maeda, R., Yano, M., Kitano, S., Miyachi, H., Fukuda, M., Shinkai, Y., and Tachibana, M. (2020). H3K9 Demethylases JMJD1A and JMJD1B Control Prospermatogonia to Spermatogonia Transition in Mouse Germline. Stem Cell Reports *15*, 424–438. https://doi.org/10.1016/j.stemcr.2020.06.013.

11. Song, H.W., Bettegowda, A., Lake, B.B., Zhao, A.H., Skarbrevik, D., Babajanian, E., Sukhwani, M., Shum, E.Y., Phan, M.H., Plank, T.D.M., et al. (2016). The Homeobox Transcription Factor RHOX10 Drives Mouse Spermatogonial Stem Cell Establishment. Cell Rep. *17*, 149–164. https://doi.org/10.1016/j.celrep.2016.08.090.

12. Du, G., Oatley, M.J., Law, N.C., Robbins, C., Wu, X., and Oatley, J.M. (2021). Proper timing of a quiescence period in precursor prospermatogonia is required for stem cell pool establishment in the male germline. Development *148*, dev194571. https://doi.org/10.1242/dev.194571.

13. Xu, J., Wan, P., Wang, M., Zhang, J., Gao, X., Hu, B., Han, J., Chen, L., Sun, K., Wu, J., et al. (2015). AIP1-mediated actin disassembly is required for postnatal germ cell migration and spermatogonial stem cell niche establishment. Cell Death Dis. *6*, e1818, ARTN e1818. https://doi.org/10.1038/cddis.2015.182.

14. Tan, K., Song, H.W., and Wilkinson, M.F. (2021). RHOX10 drives mouse spermatogonial stem cell establishment through a transcription factor signaling cascade. Cell Rep. *36*, 109423. https://doi.org/10.1016/j.celrep.2021.109423.

15. Du, G., Oatley, M.J., Law, N.C., Robbins, C., Wu, X., and Oatley, J.M. (2021). Proper timing of a quiescence period in precursor prospermatogonia is required for stem cell pool establishment in the male germline. Development *148*, dev194571. https://doi.org/10.1242/dev.194571.

16. Law, N.C., Oatley, M.J., and Oatley, J.M. (2019). Developmental kinetics and transcriptome dynamics of stem cell specification in the spermatogenic lineage. Nat. Commun. *10*, 2787, ARTN 2787. https://doi.org/10.1038/s41467-019-10596-0.

17. van Eekelen, C.A., Riemen, T., and van Venrooij, W.J. (1981). Specificity in the interaction of hnRNA and mRNA with proteins as revealed by in vivo cross linking. FEBS Lett. *130*, 223–226. https://doi.org/10.1016/0014-5793(81)81125-8.

18. Wang, X.L., Li, J.M., and Yuan, S.Q. (2023). Characterization of the protein expression and localization of hnRNP family members during murine spermatogenesis. Asian J. Androl. *25*, 314–321. https://doi.org/10.4103/aja202273.

19. Wen, Y., Ma, X., Wang, X., Wang, F., Dong, J., Wu, Y., Lv, C., Liu, K., Zhang, Y., Zhang, Z., and Yuan, S. (2021). hnRNPU in Sertoli cells cooperates with WT1 and is essential for testicular development by modulating transcriptional factors Sox8/9. Theranostics *11*, 10030–10046. https://doi.org/10.7150/thno.66819.

20. Tokuda, M., Kadokawa, Y., Kurahashi, H., and Marunouchi, T. (2007). CDH1 is a specific marker for undifferentiated spermatogonia in mouse testes. Biol. Reprod. *76*, 130–141. https://doi.org/10.1095/biolreprod.106.053181.

21. Goertz, M.J., Wu, Z., Gallardo, T.D., Hamra, F.K., and Castrillon, D.H. (2011). Foxo1 is required in mouse spermatogonial stem cells for their maintenance and the initiation of spermatogenesis. J. Clin. Invest. *121*, 3456–3466. https://doi.org/10.1172/Jci57984.

22. Zoch, A., Auchynnikava, T., Berrens, R.V., Kabayama, Y., Schöpp, T., Heep, M., Vasiliauskaitė, L., Pérez-Rico, Y.A., Cook, A.G., Shkumatava, A., et al. (2020). SPOCD1 is an essential executor of piRNA-directed de novo DNA methylation. Nature *584*, 635–639. https://doi.org/10.1038/s41586-020-2557-5.

23. Tan, K., Song, H.W., and Wilkinson, M.F. (2021). RHOX10 drives mouse spermatogonial stem cell establishment through a transcription factor signaling cascade. Cell Rep. *36*, 109423. https://doi.org/10.1016/j.celrep.2021.109423.

24. Zhao, J., Lu, P., Wan, C., Huang, Y., Cui, M., Yang, X., Hu, Y., Zheng, Y., Dong, J., Wang, M., et al. (2021). Cell-fate transition and determination analysis of mouse male germ cells throughout development. Nat. Commun. *12*, 6839. https://doi.org/10.1038/s41467-021-27172-0.

25. Green, C.D., Ma, Q., Manske, G.L., Shami, A.N., Zheng, X., Marini, S., Moritz, L., Sultan, C., Gurczynski, S.J., Moore, B.B., et al. (2018). A Comprehensive Roadmap of Murine Spermatogenesis Defined by Single-Cell RNA-Seq. Dev. Cell *46*, 651–667.e10. https://doi.org/10.1016/j.devcel.2018.07.025.

26. Wang, Z., Xu, X., Li, J.L., Palmer, C., Maric, D., and Dean, J. (2019). Sertoli cell-only phenotype and scRNA-seq define PRAMEF12 as a factor essential for spermatogenesis in mice. Nat. Commun. *10*, 5196. https://doi.org/10.1038/s41467-019-13193-3.

27. Guo, J., Nie, X., Giebler, M., Mlcochova, H., Wang, Y., Grow, E.J., DonorConnect; Kim, R., Tharmalingam, M., Matilionyte, G., et al. (2020). The Dynamic Transcriptional Cell Atlas of Testis Development during Human Puberty. Cell Stem Cell *26*, 262–276.e4. https://doi.org/10.1016/j.stem.2019.12.005.

28. Suzuki, S., McCarrey, J.R., and Hermann, B.P. (2021). An mTORC1-dependent switch orchestrates the transition between mouse spermatogonial stem cells and clones of progenitor spermatogonia. Cell Rep. *34*, 108752. https://doi.org/10.1016/j.celrep.2021.108752.

29. Yang, D., Lu, Q., Peng, S., and Hua, J. (2023). Ubiquitin C-terminal hydrolase L1 (UCHL1), a double-edged sword in mammalian oocyte maturation and spermatogenesis. Cell Prolif. *56*, e13347. https://doi.org/10.1111/cpr.13347.

30. Xiao, R., Tang, P., Yang, B., Huang, J., Zhou, Y., Shao, C., Li, H., Sun, H., Zhang, Y., and Fu, X.D. (2012). Nuclear Matrix Factor hnRNP U/SAF-A Exerts a Global Control of Alternative Splicing by Regulating U2 snRNP Maturation. Mol. Cell *45*, 656–668. https://doi.org/10.1016/j.molcel.2012.01.009.

31. Ye, J., Beetz, N., O'Keeffe, S., Tapia, J.C., Macpherson, L., Chen, W.V., Bassel-Duby, R., Olson, E.N., and Maniatis, T. (2015). hnRNP U protein is required for normal pre-mRNA splicing and postnatal heart development and function. Proc. Natl. Acad. Sci. USA *112*, E3020–E3029. https://doi.org/10.1073/pnas.1508461112.

32. Li, H., Liang, Z., Yang, J., Wang, D., Wang, H., Zhu, M., Geng, B., and Xu, E.Y. (2019). DAZL is a master translational regulator of murine spermatogenesis. Natl. Sci. Rev. *6*, 455–468. https://doi.org/10.1093/nsr/nwy163.

33. Choi, Y.H., Park, C.H., Kim, W., Ling, H., Kang, A., Chang, M.W., Im, S.K., Jeong, H.W., Kong, Y.Y., and Kim, K.T. (2010). Vaccinia-Related Kinase 1 Is Required for the Maintenance of Undifferentiated Spermatogonia in Mouse Male Germ Cells. PLoS One *5*, e15254. https://doi.org/10.1371/journal.pone.0015254.

34. Holloway, J.K., Mohan, S., Balmus, G., Sun, X., Modzelewski, A., Borst, P.L., Freire, R., Weiss, R.S., and Cohen, P.E. (2011). Mammalian BTBD12 (SLX4) Protects against Genomic Instability during Mammalian Spermatogenesis. PLoS Genet. *7*, e1002094, ARTN e1002094. https://doi.org/10.1371/journal.pgen.1002094.

35. Puri, P., Phillips, B.T., Suzuki, H., Orwig, K.E., Rajkovic, A., Lapinski, P.E., King, P.D., Feng, G.S., and Walker, W.H. (2014). The Transition from Stem Cell to Progenitor Spermatogonia and Male Fertility Requires the SHP2 Protein Tyrosine Phosphatase. Stem Cells *32*, 741–753. https://doi.org/10.1002/stem.1572.

36. Legrand, J.M.D., Chan, A.L., La, H.M., Rossello, F.J., Änkö, M.L., Fuller-Pace, F.V., and Hobbs, R.M. (2019). DDX5 plays essential transcriptional and post-transcriptional roles in the maintenance and function of spermatogonia. Nat. Commun. *10*, 2278, ARTN 2278. https://doi.org/10.1038/s41467-019-09972-7.

37. Xia, Q., Cui, G., Fan, Y., Wang, X., Hu, G., Wang, L., Luo, X., Yang, L., Cai, Q., Xu, K., et al. (2021). RNA helicase DDX5 acts as a critical regulator for survival of neonatal mouse gonocytes. Cell Prolif. *54*, e13000, ARTN e13000. https://doi.org/10.1111/cpr.13000.

38. Matson, C.K., Murphy, M.W., Griswold, M.D., Yoshida, S., Bardwell, V.J., and Zarkower, D. (2010). The Mammalian Doublesex Homolog DMRT1 Is a Transcriptional Gatekeeper that Controls the Mitosis versus Meiosis Decision in Male Germ Cells. Dev. Cell *19*, 612–624. https://doi.org/10.1016/j.devcel.2010.09.010.

39. Do, D.V., Strauss, B., Cukuroglu, E., Macaulay, I., Wee, K.B., Hu, T.X., Igor, R.D.L.M., Lee, C., Harrison, A., Butler, R., et al. (2018). SRSF3 maintains transcriptome integrity in oocytes by regulation of alternative splicing and transposable elements. Cell Discov. *4*, 33, ARTN 33. https://doi.org/10.1038/s41421-018-0032-3.

40. Song, X., Wan, X., Huang, T., Zeng, C., Sastry, N., Wu, B., James, C.D., Horbinski, C., Nakano, I., Zhang, W., et al. (2019). SRSF3-Regulated RNA Alternative Splicing Promotes Glioblastoma Tumorigenicity by Affecting Multiple Cellular Processes. Cancer Res. *79*, 5288–5301. https://doi.org/10.1158/0008-5472.Can-19-1504.

41. Tan, J.H.L., Wollmann, H., van Pelt, A.M.M., Kaldis, P., and Messerschmidt, D.M. (2020). Infertility-Causing Haploinsufficiency Reveals TRIM28/KAP1 Requirement in Spermatogonia. Stem Cell Reports *14*, 818–827. https://doi.org/10.1016/j.stemcr.2020.03.013.

42. Busada, J.T., Kaye, E.P., Renegar, R.H., and Geyer, C.B. (2014). Retinoic Acid Induces Multiple Hallmarks of the Prospermatogonia-to-Spermatogonia Transition in the Neonatal Mouse. Biol. Reprod. *90*, 64, ARTN 64. https://doi.org/10.1095/biolreprod.113.114645.

43. Roosen-Runge, E.C., and Leik, J. (1968). Gonocyte degeneration in the postnatal male rat. Am. J. Anat. *122*, 275–299. https://doi.org/10.1002/aja.1001220208.

44. Guo, J., Grow, E.J., Mlcochova, H., Maher, G.J., Lindskog, C., Nie, X., Guo, Y., Takei, Y., Yun, J., Cai, L., et al. (2018). The adult human testis transcriptional cell atlas. Cell Res. *28*, 1141–1157. https://doi.org/10.1038/s41422-018-0099-2.

45. Guo, J., Grow, E.J., Yi, C., Mlcochova, H., Maher, G.J., Lindskog, C., Murphy, P.J., Wike, C.L., Carrell, D.T., Goriely, A., et al. (2017). Chromatin and Single-Cell RNA-Seq Profiling Reveal Dynamic Signaling and Metabolic Transitions during Human Spermatogonial Stem Cell Development. Cell Stem Cell *21*, 533–546.e6. https://doi.org/10.1016/j.stem.2017.09.003.

46. Guo, J., Sosa, E., Chitiashvili, T., Nie, X., Rojas, E.J., Oliver, E., DonorConnect; Plath, K., Hotaling, J.M., Stukenborg, J.B., et al. (2021). Single-cell analysis of the developing human testis reveals somatic niche cell specification and fetal germline stem cell establishment. Cell Stem Cell *28*, 764–778.e4. https://doi.org/10.1016/j.stem.2020.12.004.

47. Tan, K., and Wilkinson, M.F. (2020). A single-cell view of spermatogonial stem cells. Curr. Opin. Cell Biol. *67*, 71–78. https://doi.org/10.1016/j.ceb.2020.07.005.

48. Murat, F., Mbengue, N., Winge, S.B., Trefzer, T., Leushkin, E., Sepp, M., Cardoso-Moreira, M., Schmidt, J., Schneider, C., Mößinger, K., et al. (2023). The molecular evolution of spermatogenesis across mammals. Nature *613*, 308–316. https://doi.org/10.1038/s41586-022-05547-7.

49. Feng, S., Li, J., Wen, H., Liu, K., Gui, Y., Wen, Y., Wang, X., and Yuan, S. (2022). hnRNPH1 recruits PTBP2 and SRSF3 to modulate alternative splicing in germ cells. Nat. Commun. *13*, 3588. https://doi.org/10.1038/s41467-022-31364-7.

50. Manku, G., Mazer, M., and Culty, M. (2012). Neonatal testicular gonocytes isolation and processing for immunocytochemical analysis. Methods Mol. Biol. *825*, 17–29. https://doi.org/10.1007/978-1-61779-436-0_2.

51. Dong, J., Wang, X., Cao, C., Wen, Y., Sakashita, A., Chen, S., Zhang, J., Zhang, Y., Zhou, L., Luo, M., et al. (2019). UHRF1 suppresses retrotransposons and cooperates with PRMT5 and PIWI proteins in male germ cells. Nat. Commun. *10*, 4705. https://doi.org/10.1038/s41467-019-12455-4.

52. Butler, A., Hoffman, P., Smibert, P., Papalexi, E., and Satija, R. (2018). Integrating single-cell transcriptomic data across different conditions, technologies, and species. Nat. Biotechnol. *36*, 411–420. https://doi.org/10.1038/nbt.4096.

53. Qiu, X., Mao, Q., Tang, Y., Wang, L., Chawla, R., Pliner, H.A., and Trapnell, C. (2017). Reversed graph embedding resolves complex single-cell trajectories. Nat. Methods *14*, 979–982. https://doi.org/10.1038/nmeth.4402.

54. Zhou, Y., Zhou, B., Pache, L., Chang, M., Khodabakhshi, A.H., Tanaseichuk, O., Benner, C., and Chanda, S.K. (2019). Metascape provides a biologist-oriented resource for the analysis of systems-level datasets. Nat. Commun. *10*, 1523. https://doi.org/10.1038/s41467-019-09234-6.

STAR★METHODS

KEY RESOURCES TABLE

REAGENT or RESOURCE	SOURCE	IDENTIFIER
Antibodies		
Mouse- anti-PLZF	Santa	SC-28391
Rabbit- anti-SCP3	Abcam	ab15093
Mouse- anti-γ-H2AX	Abcam	ab26350
Rabbit - anti-DDX4	Abcam	ab13840
Rabbit - anti-STRA8	Millipore	ABN1656
Rat - anti-TRA98	Abcam	ab82527
Rabbit - anti-WT1	Abcam	Ab89901
Rabbit - anti-KI67	Abcam	ab15580
Mouse - anti-hnRNPU	Santa	sc-32315
Rabbit - anti-hnRNPU	Abclonal	A3917
Rabbit - anti-FOXO1	CST	C29H4
Rabbit- anti-DNMT3L	Abcam	Ab194094
Rabbit- anti-E-cadherin	Proteintech	20874-1-AP
Rabbit- anti-DDX5	Huabio	ET1705-32
Rabbit- anti-TRIM28	Huabio	R1210-2
Rabbit- anti-SRSF3	Abclonal	A9054
Goat- anti-cKIT	RD	AF1356
Rabbit- anti-ETV4	Proteintech	10684-1-AP
Rabbit- anti-MIWI2	home-made	Gift from Dr. Deqiang Ding
Goat- anti-GFRa1	RD	AF560
Rabbit - anti- Histone-H3	Proteintech	17168-1-AP
Rabbit- anti-GAPDH	Proteintech	10494-1-AP
IFKine™ Green Donkey Anti-Mouse IgG	Abbkine	A24211
IFKine™ Red Donkey Anti-Mouse IgG	Abbkine	A24411
IFKine™ Green Donkey Anti-Rabbit IgG	Proteintech	A24221
IFKine™ Red Donkey Anti-Rabbit IgG	Abbkine	A24421
IFKine™ Green Donkey Anti-Goat IgG	Abbkine	A24231
HRP Goat anti-rabbit IgG	Abbkine	A21020
HRP Goat anti-mouse IgG	Abbkine	A21010
Chemicals, peptides, and recombinant proteins		
NaCl	Sinopharm	10019318
protease inhibitor cocktail	MCE	HY-K0010
Critical commercial assays		
PBS	Servicebio	G4202
IP lysis buffer	Beyotime	P0013
protein A/G magnetic beads	MCE	HY-K0202
RNase A	Beyotime	ST578
5×SDS-PAGE protein loading buffer	Yeasen	20315ES20
skim milk	Biosharp	BS102
ECL reagent mixture	Bio-Rad	1705061
antifade mounting medium	Abbkine	BMU104-CN
Bouin's solution	Sigma-Aldrich	HT10132
Periodic Acid-Schiff Staining Kit	Beyotime	C0142S

(*Continued on next page*)

Continued		
REAGENT or RESOURCE	SOURCE	IDENTIFIER
O.C.T.	Sakura Finetek	4583
Deposited data		
sc-RNA-seq	This paper	NCBI database: PRJNA896932 PRJNA897864
RIP-seq	This paper	NCBI database: PRJNA1058363
Experimental models: Organisms/strains		
floxed-Hnrnpu mice	A gift from Dr. Tom Maniatis at Columbia University College of Physicians and Surgeons	N/A
Vasa-Cre mice	The Jackson Laboratory	RRID:IMSR_JAX:006954
Ddx4-Cre^{ERT2} mice	The Jackson Laboratory	RRID:IMSR_JAX:024760
Oligonucleotides		
List of Oligonucleotides used	This study	Table S6
Software and algorithms		
Metascape	https://metascape.org/	N/A
STRING	https://cn.string-db.org/	N/A
Photoshop	Adobe	N/A
Prism	GraphPad	N/A
Image J	NIH	https://imagej.nih.gov/ij/
exomePeak Version 3.8	N/A	N/A
deepTools Version 2.4.1	N/A	N/A
Biorender	https://app.biorender.com/	N/A

RESOURCE AVAILABILITY

Lead contact

Further information and requests for resources and reagents should be directed to and will be fulfilled by the lead contact, Dr. Shuiqiao Yuan (shuiqiaoyuan@hust.edu.cn).

Materials availability

Reagents describe in this paper are available from the lead contact upon request with a completed Material Transfer Agreement.

Data and code availability

- RNA-seq, scRNA-seq, and RIP-seq data have been deposited in the NCBI SRA (Sequence Read Achieve) database and are publicly available. Accession numbers are listed in the key resources table.
- The codes used for analysis in this study are available at GitHub repository: https://github.com/chengkeren/hnRNPU.
- Any additional information required to reanalyze the data reported in this work paper is available from the lead contact upon request.

EXPERIMENTAL MODEL AND STUDY PARTICIPANT DETAILS

Generation of *Hnrnpu* gene conditional knockout mice

Mice carrying floxed hnRNPU alleles were a gift from Dr. Tom Maniatis's lab at Columbia University and have been previously described.[19] The *Vasa*-Cre and *Ddx4*-Cre^{ERT2} mice were purchased from Jackson Laboratory. Vasa-Cre-CKO (*Vasa*-Cre; *Hnrnpu*$^{flox/Del}$) were obtained by matting female *Hnrnpu*$^{flox/flox}$ mice with *Vasa*-Cre; *Hnrnpu*$^{+/flox}$ male mice. hnRNPU-*iKO* (*DDX4*-Cre^{ERT2}; *Hnrnpu*$^{flox/flox}$) mice were obtained by matting female *Hnrnpu*$^{flox/flox}$ mice with *Ddx4*-Cre^{ERT2}; *Hnrnpu*$^{flox/flox}$ male mice. For inducible deletion of *Hnrnpu* in *iKO* mice, tamoxifen (Sigma T5648) was suspended with corn oil (Sigma C8267) and injected intraperitoneally daily into 8-week-old *Ddx4*-Cre^{ERT2}; *Hnrnpu*$^{flox/flox}$ males (2mg / 30g body weight) for 5 consecutive days. *Hnrnpu*$^{flox/flox}$ males treated with tamoxifen were used as controls. Testes were harvested for analysis at 35 days post-tamoxifen treatment (dpt). The PCR primer sequences for genotyping are listed in Table S6.

Animal

All mice used in this study were C57BL/6J gene background and housed in a specific pathogen-free (SPF) conditions at 20-26°C and 40-70% humidity in the Laboratory Animal Center of Tongji Medical College, Huazhong University of Science and Technology, China. All animal experiments were approved by the Institutional Animal Care and Use Committee (IACUC) of Tongji Medical College. Y.W. and L.Y. were responsible for the feeding of mice.

Human testicular samples

Human testicular samples were obtained from aborted fetuses and obstructive azoospermia patients. All experiments were conducted following the protocols approved by the Medical Ethics Committee of the Reproductive Medicine Center of Tongji Medical College of Huazhong University of Science and Technology. All participating patients consented to the research process for this work and granted this permission with informed written authorization.

METHOD DETAILS

Purification of spermatogenic cells, Sertoli cells, and neonatal germ cells

STA-PUT velocity sedimentation was used to separate different types of germ cells as we have previously described, including spermatogonia, pachytene spermatocytes, round spermatids, and elongating spermatids.[49] To obtain single testicular cell suspension, mouse testes at P56 were treated with collagenase IV (Sigma, Cat. No. C5138-100 mg) and trypsin (Sigma, Cat. No. 9002-07-7). After washing with PBS, the heterogeneous testicular cell suspension was filtered and dispersed in a linear BSA gradient in a group of specialized glassware. The sedimentation velocity of individual cell types varies with cell size, enabling fractions enriched for specific cell types to be collected. The isolated spermatogenic cells with $\geq$90% purity were used for RT-qPCR analyses.

Sertoli cell isolation was performed as described previously.[19] In brief, the testes were decapsulated and digested into single-cell suspension, and then testicular cell suspension was cultured in the DMEM/F12 medium containing 10% FBS and 1% P/S. After overnight culture, the suspended cells and non-attached cells were removed by Tris-HCl (PH = 7.4) solution. Then the firmly attached Sertoli cells were digested from the cell culture dish for subsequent experiments.

For the neonatal testicular germ cell purification, more than 100 neonatal mouse testes were obtained from P4 mice and dissociated with single cells as previously described.[50] In short, testicular cells were collected by two-step enzymatic digestion. Testicular samples were digested with collagenase IV (1 mg/ml), washed with PBS, and centrifuged at 500 g. Then, the pellet was digested again with trypsin containing DNase I (1mg/ml) to prepare a single-cell suspension. Then the single-cell suspension was plated on 0.1% gelatin-coated plates and incubated overnight. During overnight plating, somatic cells adhered to the culture plates and germ cells remained non-attached. The next day, germ cells were enriched by gelatin selection by collecting the non-attached cells. Germ cells were judged by morphology and larger size compared to Sertoli cells by phase contrast microscopy. In addition, fractions containing germ cells were centrifuged and collected for immunoprecipitation, RNA immunoprecipitation, and RNA extraction.

Histology and immunofluorescence

Mouse testes and epididymides were fixed in Bouin's solution (Lot#SLBJ3855V, Sigma) or 4% paraformaldehyde (PFA) solution (Sigma, P6148) overnight at 4°C with tilting and rotation. For histology analyses, the samples were dehydrated in ethanol and embedded in paraffin. 5 μm sections were cut and stained with a periodic acid-Schiff (PAS) kit according to the manufacturer's instructions. Immunofluorescence assay was performed as described previously with minor modifications.[51] Briefly, the cryosections were subjected to antigen retrieval and blocked with 5% donkey serum for 1h at RT. Then, the sections were incubated with primary antibodies overnight at 4°C and incubated with secondary antibodies for 1-2h at RT. After being washed with PBS, sections were mounted with Vectashield mounting medium containing DAPI (H1200, Vector laboratories) and imaged using a Zeiss Axio Scope.A1 microscope (Zeiss, Germany) equipped with a digital camera (MSX2, Micro-shot Technology Limited, China).

For whole-mount staining, freshly isolated seminiferous tubules were fixed in 4% PFA and 0.5 mM $CaCl_2$ overnight at 4°C, dehydrated in a graded ethanol series (25%, 50%, 75%, and 100%) in PBST at 4°C. After rehydrating in PBST, the seminiferous tubules were permeabilized in blocking buffer containing 4% donkey serum and 1% BSA in PBST for 1 h at RT and then incubated with primary antibodies overnight at 4°C. Secondary antibodies conjugated to Alexa Fluor Dyes were incubated with seminiferous tubules for 1 h at RT. After washing in PBST, the seminiferous tubules were stained with DAPI and mounted with PBS on the slides. Then fluorescent images were captured using a Zeiss Axio Scope.A1 microscope (Zeiss, Germany) equipped with a digital camera (MSX2, Micro-shot Technology Limited, China). The antibodies used are listed in the key resources table in the STAR Methods.

TUNEL analyses

TUNEL assay was performed with One Step TUNEL Apoptosis Assay Kit (Meilunbio, MA0223) following the manufacturer's instructions using testis cryosections.

Chromatin fractionation

Testes were harvested from control and Vasa-Cre-cKO mice at P5 and used for chromatin fractionation assay according to the manufacturer's procedure (Beyotime, P0027). Briefly, testes were homogenized thoroughly and stewed in the mixture of buffer A and B at

4°C. After centrifugation at 1,500g for 5 min at 4°C, the supernatant containing the cytoplasm was transferred to a cold tube, while the sediment was vortexed vigorously in buffer A and then placed on ice for 15 min. Buffer B was added to the suspension, and after two vigorous vortices and one centrifugation, the supernatant was transferred to the tube containing cytoplasm. To obtain chromatin proteins, the sediment was rinsed in the nuclear protein extraction reagent with the addition of PMSF and vortexed at high speed for 15-30s every 1-2 min for a total of 30 min. After centrifugation at 16,000g for 10 min at 4°C, the supernatant containing nuclear proteins was transferred to a cold tube for subsequent experiments.

Western blotting

Testes were removed from the tunica albuginea and lysed with RIPA buffer (CWBIO, Cat# 01408) plus 1× proteinase inhibitor in a 1.5 ml Eppendorf tube. The lysates were sonicated and clarified by centrifugation, analyzed on SDS/PAGE gel, and followed by electroblotted onto PVDF membrane (Bio-Rad). The membranes were incubated with primary antibody diluted with 5% non-fat milk and were probed with secondary antibody immediately at RT for 1-2 h. The signals were visualized using the Luminol/enhancer solution and Peroxide solution (ClarityTM Western ECL Substrate, Bio-Rad) and photographed using the ChemiDoc XRS+ system (Bio-Rad). The antibodies used are listed in the key resources table in the STAR Methods. All original uncropped gels of Western blotting are shown in Data S1.

Immunoprecipitation

Isolated germ cells were used were homogenized in iced lysis buffer (20 mM HEPES, 150 mM NaCl, 2 mM magnesium acetate, 0.2% NP-40, 1 mM DTT, pH = 7.3) and were then clarified by centrifugation at 12,000 X g. Immunoprecipitation was performed using Protein A beads or Protein G beads (Bio-Rad) according to the manufacturer's instructions, and western blots were performed according to the above western blotting protocols. 10 μg of antibody was used for each experiment. The antibodies used are listed in the key resources table in the STAR Methods.

Quantitative real-time PCR (RT-qPCR)

Total RNA was prepared from testes using TRIzol reagent (Invitrogen, 15596-025) following the manufacturer's procedure. For microcellular RNA extraction and reverse transcription: RNA from isolated germ cells from neonatal control and Vasa-Cre-cKO testes were extracted and reverse transcribed using a single-cell sequence-specific amplification kit (P621, Vazyme). The operation steps are carried out under the manufacturer's instructions. qRT-PCR was performed using SYBR green master mix with gene-specific primer sets in a Step One Plus machine (Applied Biosystems, 4309155) on an equal amount of total RNA from testes of each genotype and analyzed using the $2^{-\Delta\Delta Ct}$ method with GAPDH as an internal control. The primers used are listed in Table S6.

RNA-immunoprecipitation and sequencing analyses

Spermatogonia were roughly isolated from 40 testes from P5 mice and homogenized in ice-cold lysis buffer (50mM Tris-HCl pH 7.4, 100mM NaCl, 0.5% NP-40, 1:100 protease inhibitors cocktail, RNase inhibitor). After incubating on ice for 20 min to lysis the cell, the lysate was centrifuged at 15,000g for 10 min at 4°C. The 10% lysis sample was stored for "input", and the remaining was used in immunoprecipitation reactions with an anti-hnRNPU antibody and rabbit IgG, respectively. The RNA of input and RIP was extracted using TRIzol reagent (Invitrogen). KC-Digital™ Stranded mRNA Library Prep Kit for Illumina® was used to construct the stranded RNA sequencing library following the manufacturer's instructions. The Kit eliminates duplication bias in PCR and sequencing by using a unique molecular identifier (UMI) to label the pre-amplified cDNA molecules. The library products corresponding to 200 bps were enriched, quantified, and sequenced on a Novaseq 6000 sequencer (Illumina) with a PE150 model.

Trim-galore was used to filter the raw sequencing data, discarding low-quality reads and trimming reads contaminated with adaptor sequences. The de-duplicated consensus sequences were mapped to the UCSC mouse genome reference (mm10) using STAR software with default parameters. Peak calling was performed using ExomePeak software, and annotation was performed using bedtools. Sequence motifs enriched in peak regions were identified using STREME_V2. Gene ontology (GO) analysis for annotated genes was performed using Metascape with a corrected *P*-value cutoff of 0.05 to assess statistically significant enrichment. The primers used are listed in Table S6.

RNA-seq and analyses

Total RNAs were extracted from P4 control and Vasa-Cre-cKO mice using TRIzol reagent (Invitrogen). Then, a total amount of 2 μg of RNA per sample was used to prepare mRNA libraries using TruSeq Stranded mRNA Library Preparation Kit Set A (Cat. No. RS-122-2101, Illumina) according to the manufacturer's instructions and base pairs (raw data) were generated by the Illumina HiSeq 4000 platform. The FASTX-Toolkit was used to remove adaptor sequences, and low-quality reads from the sequencing data. Then we used Tophat2 and Cufflinks to assemble the sequencing reads based on the UCSC MM10 mouse genome.

rMATS was used to analyze the alternative splicing events between control and Vasa-Cre-cKO testes. To detect valid alternative splicing events, those with a false discovery rate (FDR) <0.05 and $|\triangle PSI| > 10\%$ were categorized as differential alternative splicing events based on raw read counts.

To predict APA events, the quantification of APA (QAPA) algorithm, a faster and more sensitive approach to quantitatively infer APA from conventional RNA-seq data based on a greatly expanded resource of poly(A) site annotations, was used to verify APA events

predicted by DaPars. Distal poly(A) site usage (DPAU) was defined as the relative expression of distal 3′UTR isoforms to the total expression of all detected 3′UTR isoforms. The median change in DPAU (ΔDPAU, DN-control) between DN and control was calculated. Genes with ΔDPAU > 10 and P-value $\leq$ 0.05 were deemed to have lengthening 3′UTRs, while ΔDPAU < −10 and P-value $\leq$ 0.05 were considered as 3′UTRs shortening.

Single-cell RNA-seq analyses

For the preparation of single-cell suspensions, testes at P5 were digested in a collagenase solution comprising 1 mg/mL collagenase IV (Sigma, Cat. No. C5138-100 mg) in RPMI1640 medium at 37°C on a shaker for 15 min. Then the loosened seminiferous tubules were further digested in trypsin solution comprising 2.5 mg/ml trypsin-EDTA and 0.5 mg/mL Deoxyribonuclease I in RPMI1640 medium with occasional pipetting at 37°C for 10 min. The cell suspension was then filtered with a 40 μm pore-size nylon mesh and centrifuged at 300 g for 10 min at 4°C. Subsequently, testicular cells were sorted into PBS following the 10× Genomics protocol. The resulting cell suspension was loaded into a Chromium Controller (10x Genomics), and single-cell cDNA libraries were then constructed using Chromium Single Cell 3′ Reagent kits (v2) following the manufacturer's protocols. The libraries were quantified by digital PCR and subjected to 150 bp paired-end sequencing on an Illumina NovaSeq 6000 platform (Illumina). Raw base call files were demultiplexed using the 10x Genomics Cell Ranger pipeline and aligned to the mouse mm10 transcriptome. Raw gene expression matrices were imported into R (version 4.1.2). Seurat package was used for cell filtration, normalization of data, reduction of dimensionality reduction, cell cluster, and differentially expressed gene identified.[52] Cells with less than 200 genes and more than 8000 genes or mitochondrial genes of more than 15 were excluded for subsequent data analysis. 'FindVariableFeatures' was used to identify the top 2000 most hypervariable genes, and these genes were selected for principal component analysis (PCA) and linear dimension reduction. The original Louvain algorithm (FindClusters) with a clustering resolution of 0.5 was performed to cluster the cells. Differentially expressed genes of each sample were conducted using a Wilcoxon rank-sum test with p-value < 0.05, log(fc.threshold) = 0.25. Cell types were allocated to each cluster using the known marker genes as described previously. Monocle 2 packages were used to construct single-cell pseudotime trajectories according to the provided documentation.[53] Objects used for cell cycle score analysis were from Seurat objects that had been quality-controlled and standardized in the previous step. G1, S, and G2/M phase genes are derived from the cc.genes list of the CellCycleScoring function of Seurate (https://satijalab.org/seurat/archive/v3.1/cell_cycle_vignette.html). All single-cell data analyses were performed in the R environment. Metascape (http://metascape.org) was applied for functional enrichment analysis.[54]

QUANTIFICATION AND STATISTICAL ANALYSIS

All quantitative data are presented as mean ± SEM. Differences between experimental groups were determined statistically using one-way ANOVA or Student's t-test using the SPSS19.0 software. *P*-values are denoted in figures by $^{*}P < 0.05$; $^{**}P < 0.01$; and $^{***}P < 0.001$. Go ontology and protein-protein interaction network were analyzed online by using Metascape (https://metascape.org/) or STRING (https://cn.string-db.org/). Images and data quantitation were processed by Image J or GraphPad Prism software, respectively. Graphical abstract was created with BioRender.com.